Research Paper

GEOSPHERE

GEOSPHERE; v. 11, no. 4

doi:10.1130/GES01108.1

12 figures; 4 tables; 1 supplemental file

CORRESPONDENCE: anelson@usgs.gov

CITATION: Nelson, A.R., Briggs, R.W., Dura, T., Engelhart, S.E., Gelfenbaum, G., Bradley, L.-A., Forman, S.L., Vane, C.H., and Kelley, K.A., 2015, Tsunami recurrence in the eastern Alaska-Aleutian arc: A Holocene stratigraphic record from Chirikof Island, Alaska: Geosphere, v. 11, no. 4, p. 1172–1203, doi:10.1130/GES01108.1.

Received 24 July 2014
Revision received 23 April 2015
Accepted 11 June 2015
Published online 1 July 2015

Tsunami recurrence in the eastern Alaska-Aleutian arc: A Holocene stratigraphic record from Chirikof Island, Alaska

Alan R. Nelson[1], Richard W. Briggs[1], Tina Dura[2], Simon E. Engelhart[3], Guy Gelfenbaum[4], Lee-Ann Bradley[1], Steve L. Forman[5], Christopher H. Vane[6], and Katherine A. Kelley[7]

[1]Geologic Hazards Science Center, U.S. Geological Survey, Golden, Colorado 80401, USA
[2]Sea Level Research, Department of Marine and Coastal Science, Rutgers University, New Brunswick, New Jersey 08901, USA
[3]Department of Geosciences, University of Rhode Island, Kingston, Rhode Island 02881, USA
[4]Pacific Coastal and Marine Science Center, U.S. Geological Survey, Santa Cruz, California 95060, USA
[5]Department of Geology, Baylor University, Waco, Texas 76798-7354, USA
[6]British Geological Survey, Keyworth, Nottingham, NG12 5GG, UK
[7]Graduate School of Oceanography, University of Rhode Island, Narragansett, Rhode Island 02882, USA

ABSTRACT

Despite the role of the Alaska-Aleutian megathrust as the source of some of the largest earthquakes and tsunamis, the history of its pre–twentieth century tsunamis is largely unknown west of the rupture zone of the great (magnitude, M 9.2) 1964 earthquake. Stratigraphy in core transects at two boggy lowland sites on Chirikof Island's southwest coast preserves tsunami deposits dating from the postglacial to the twentieth century. In a 500-m-long basin 13–15 m above sea level and 400 m from the sea, 4 of 10 sandy to silty beds in a 3–5-m-thick sequence of freshwater peat were probably deposited by tsunamis. The freshwater peat sequence beneath a gently sloping alluvial fan 2 km to the east, 5–15 m above sea level and 550 m from the sea, contains 20 sandy to silty beds deposited since 3.5 ka; at least 13 were probably deposited by tsunamis. Although most of the sandy beds have consistent thicknesses (over distances of 10–265 m), sharp lower contacts, good sorting, and/or upward fining typical of tsunami deposits, the beds contain abundant freshwater diatoms, very few brackish-water diatoms, and no marine diatoms. Apparently, tsunamis traveling inland over low dunes and boggy lowland entrained largely freshwater diatoms. Abundant fragmented diatoms, and lake species in some sandy beds not found in host peat, were probably transported by tsunamis to elevations of >10 m at the eastern site. Single-aliquot regeneration optically stimulated luminescence dating of the third youngest bed is consistent with its having been deposited by the tsunami recorded at Russian hunting outposts in 1788, and with the second youngest bed being deposited by a tsunami during an upper plate earthquake in 1880. We infer from stratigraphy, ^{14}C-dated peat deposition rates, and unpublished analyses of the island's history that the 1938 tsunami may locally have reached an elevation of >10 m. As this is the first record of Aleutian tsunamis extending throughout the Holocene, we cannot estimate source earthquake locations or magnitudes for most tsunami-deposited beds. We infer that no more than 3 of the 23 possible tsunamis beds at both sites were deposited following upper plate faulting or submarine landslides independent of megathrust earthquakes. If so, the Semidi segment of the Alaska-Aleutian megathrust near Chirikof Island probably sent high tsunamis southward every 180–270 yr for at least the past 3500 yr.

INTRODUCTION

As a result of twenty-first century earthquakes of unexpected magnitude (M; e.g., 2004 M 9.2 Sumatra-Andaman; 2011 M 9.0 Tohoku-Oki, Japan), accompanied by tsunamis of unanticipated height, much has been written about the need for assessments of tsunami hazards at subduction zones (e.g., Dominey-Howes et al., 2006; Dawson and Stewart, 2007; Satake and Atwater, 2007; Shennan et al., 2009; Goto et al., 2011; Butler, 2012; Goff et al., 2012; Ryan et al., 2012a; Szczuciński et al., 2012; Satake, 2014). The most comprehensive assessments are based on earthquake and tsunami histories that span multiple cycles of strain accumulation and release on the megathrust faults of subduction zones, that is, over many hundreds to thousands of years. Even in Japan, where extensive written records of earthquakes and tsunamis extend back more than a millennium, reconstructing the history of the greatest earthquakes and tsunamis requires thorough study of coastal stratigraphic archives (e.g., Minoura et al., 2001; Witter et al., 2003; Cisternas et al., 2005; Bourgeois et al., 2006; Shennan and Hamilton, 2006; Nanayama et al., 2007; Jankaew et al., 2008; Monecke et al., 2008; Sawai et al., 2012).

One of the shortest and most incomplete histories of megathrust earthquakes and tsunamis comes from one of the longest and most seismically active subduction zones, the Alaska-Aleutian arc, extending 1600 km from southeast Alaska westward to Kamchatka (Fig. 1A; Nishenko and Jacob, 1990; Vallier et al., 1994; Carver and Plafker, 2008; Ryan et al., 2012b; Ruppert et al., 2013; Butler et al., 2014; Shennan et al., 2014b). That the Aleutian arc is capable of sending damaging tsunamis across the Pacific basin is illustrated by those produced by the series of mid-twentieth century M 8–9 ruptures in the central and eastern Aleutian arc, in 1946, 1957, 1964, and 1965 (Butler, 2012; Ross et al.,

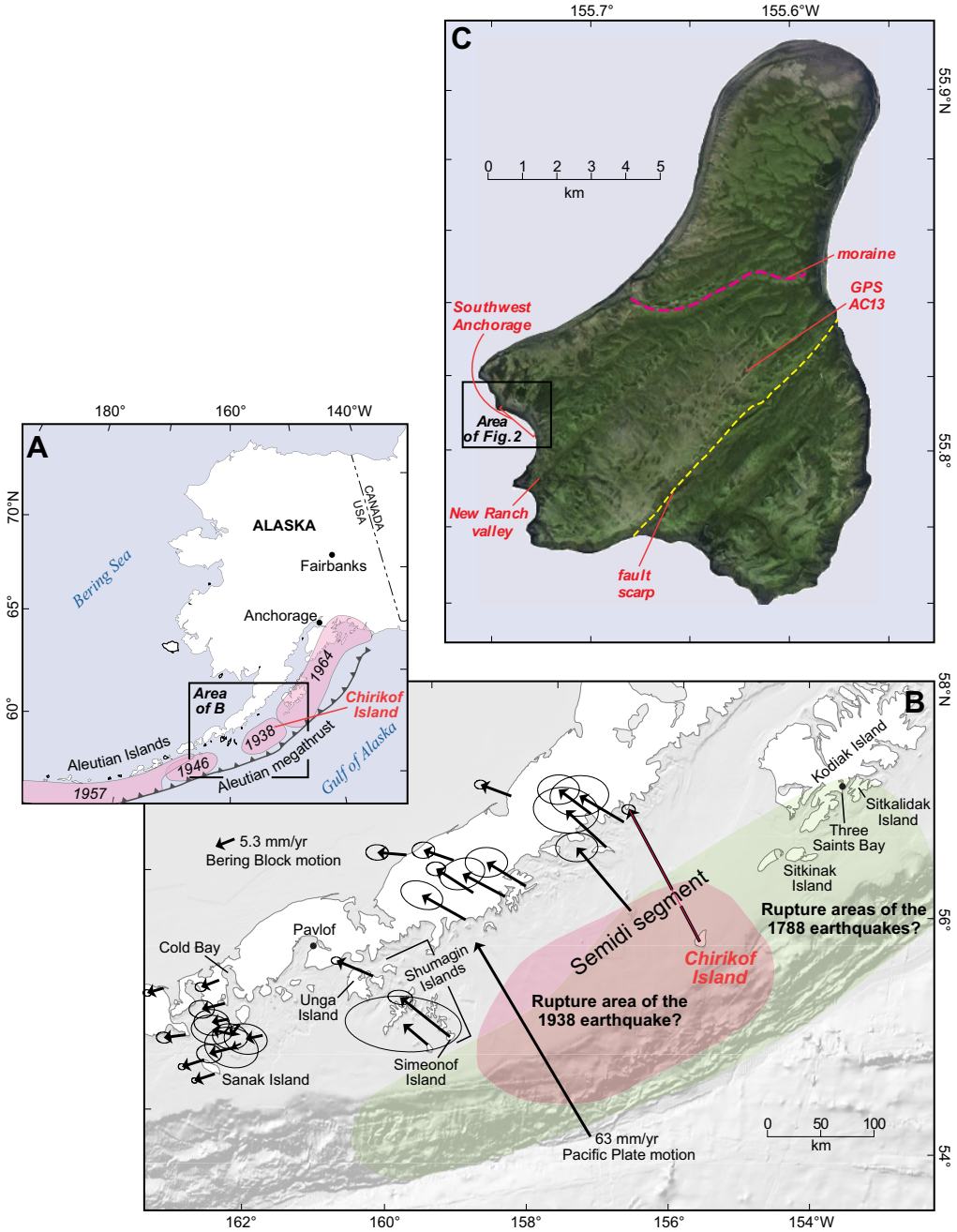

Figure 1. (A) Location of Chirikof Island within the plate tectonic setting of the Alaska-Aleutian subduction zone. Rupture areas for great twentieth century earthquakes on the megathrust are in pink. (B) Velocity field of the Alaska Peninsula and the eastern Aleutian Islands observed by global positioning system (GPS) (Fournier and Freymueller, 2007). Colors show inferred rupture areas for earthquakes in 1788 (green) and 1938 (orange). Both A and B are modified from Witter et al. (2014). The section of the megathrust between Kodiak Island and the Shumagin Islands has been referred to as the Semidi segment (e.g., Shennan et al., 2014b). (C) Physiography of Chirikof Island (Google Earth image, 2012) showing the location of our study area at Southwest Anchorage, a prominent moraine, a fault scarp (facing southeast) that probably records the 1880 earthquake, the New Ranch valley reconnaissance core site, and UNAVCO GPS station AC13 (http://pbo.unavco.org/station/overview/AC13). In the eighteenth and nineteenth centuries, Chirikof Island was known to native Alutiiq and Russians as Ukamuk Island.

2013). Based on historical records, a tsunami-source statistical analysis shows that the source contributing the most to the tsunami hazard for Los Angeles (peak wave height for a 475 yr return period), as well as much of the coast of California, is the eastern Aleutian arc (Thio et al., 2010; Ross et al., 2013). Prior to the twentieth century, sparse anecdotal accounts of strong shaking and tsunamis come from a few Russian hunting outposts beginning in the late eighteenth century (Davies et al., 1981; Lander, 1996; Black et al., unpublished manuscript described in the Supplemental File[1]). Comparisons with other subduction zones suggest that an earthquake of M 9.0–9.3 with a tsunami comparable to those produced during the 1960 M 9.5 Chile and 1964 M 9.2 Alaska earthquakes is plausible for the eastern arc west of Kodiak Island (McCaffrey, 2008; Butler, 2012; Ross et al., 2013).

Here we report stratigraphic, microfossil, ^{14}C age, and historical data from the closest land to the megathrust along this part of the arc: Chirikof Island (Fig. 1), the site of the first of a trio of eastern Aleutian studies directed at estimating the recurrence of prehistoric high tsunamis through study of their deposits. Companion studies by Briggs et al. (2014a) and Witter et al. (2014) focused on the history of earthquake related land-level change on Sitkinak and Simeonof Islands, 125 and 250 km to the east and west, respectively, of Chirikof Island (Fig. 1B). These earthquake and tsunami histories—combined with studies of present-day upper plate deformation from global positioning system (GPS) data (Freymueller et al., 2008)—demonstrate the variability and complexity of megathrust ruptures in this part of the arc. Although an initial stratigraphic reconnaissance, our ^{14}C-dated record from the southwest coast of Chirikof Island spans the Holocene. As ours is the first long record of prehistoric Aleutian tsunamis, we cannot estimate source earthquake locations or magnitude for most of the tsunami-deposited beds that we identify, nor can we determine what proportions of beds were deposited by tsunamis caused by upper plate faulting or submarine landslides near Chirikof Island that resulted in minimal inundation beyond the region. We argue that the proportion of non-megathrust-related tsunamis is probably small, and that this part of the arc sent high tsunamis southward every 180–270 yr for at least the past 3500 yr.

SETTING AND GEOMORPHOLOGY

Southwest Anchorage on Chirikof Island

The windswept, muskeg (boggy lowland) and grass-covered ridges and valleys of Chirikof Island (Fig. 1) are underlain by Pliocene sandstone and siltstone (Tugidak Formation), covered by thick Pleistocene glacial sediment in the island's northern third, and by Oligocene continental and marine clastic rocks overlain by thin drift in its southern two-thirds, where resistant conglomerates form dramatic headlands (Moore in the Supplemental File [see footnote 1]; Cohee et al., 1969; Nilsen and Moore, 1979). A 500-m-wide moraine traverses the island from west to east (Fig. 1C; Workman, 1969; Saltonstall and Steffian in the Supplemental File [see footnote 1]). Radiocarbon ages and core stratigraphy reported here show that the southwest coast of the island has been glaciated, but was ice free by 13.4 ka. Strong earthquakes in the Chirikof Island region, the ground motions and/or tsunamis of which reportedly affected the island, include those in 1788, 1826, 1833, 1847, 1848, 1880, 1938, and 1964 (Davies et al., 1981; Soloviev, 1990; Lander, 1996; Moore in the Supplemental File [see footnote 1]; Black et al. in the Supplemental File [see footnote 1]). Archeological surveys in 1962, 1963, 2005, and 2013 commented on the rapid erosion of coastal archaeological sites by wind, waves, and artifact hunters, exacerbated through trampling by feral cattle introduced late in the nineteenth century (Keithahn, 1962; Workman, 1966; Chaffin et al., 1983; Saltonstall and Steffian in the Supplemental File [see footnote 1]; Clark in the Supplemental File [see footnote 1]; MacNeil et al., 2007).

Our study area at Southwest Anchorage on the southwest coast of the island consists of broad, southwest-facing valleys fronted by sandy, driftwood-rich beach berms and low dunes (Fig. 1C; Fig. S1 in the Supplemental File [see footnote 1]). Our study sites in these valleys (Figs. 2 and 3) were 400–1300 m inland from the berms at present-day elevations above 7 m (survey methods described in Supplemental File [see footnote 1]) and underlain by meters of muskeg or bog peat in which the sandy deposits of tsunamis should be distinct. Planar wavecut bedrock platforms, 100–500 m wide and a few meters below mean lower low water (MLLW), lie seaward of the northwestern part of the beach at Southwest Anchorage. The site of Ukamuk village, a nineteenth century Alutiiq-Russian hunting outpost was near the southeast shore of West Lake (Fig. 2; Black et al. in the Supplemental File [see footnote 1]; Clark in the Supplemental File [see footnote 1]; Clark, 2010). We informally call the basin in the valley 500 m to the east of West Lake, Drained Lake basin. A lake that partially filled the basin at least until 1893 (Keithahn, 1962) probably drained early in the twentieth century.

Land-Level Changes During Earthquake Cycles

From Chirikof Island's proximity to the Alaska-Aleutian megathrust trench (100 km), we infer that it rose and fell during earthquake cycles on the subduction-zone megathrust, like similarly situated islands at this and other subduction zones (e.g., Briggs et al., 2006; Sauber et al., 2006; Melnick et al., 2012). The Plate Boundary Observatory (UNAVCO EarthScope project, pbo.unavco.org/) GPS instrument (station AC13, Fig. 1C) shows that Chirikof Island has been subsiding ~11 mm/yr since 2008 (http://pbo.unavco.org/station/overview/AC13; Fig. S1 in the Supplemental File [see footnote 1]), as would be expected if the plate boundary beneath the island were accumulating strain to be released in a future earthquake. Geodetic coupling models imply that the megathrust beneath Chirikof Island is 90%–100% locked (Fournier and Freymueller, 2007).

A few anecdotal observations show that parts of Chirikof Island rose and fell during an earthquake in 1880. A report of a creek on the south side of the island that was wider, deeper, and saltier following the 1880 earthquake (Lander, 1996, p. 46) suggests a few decimeters of subsidence about the time of the earth-

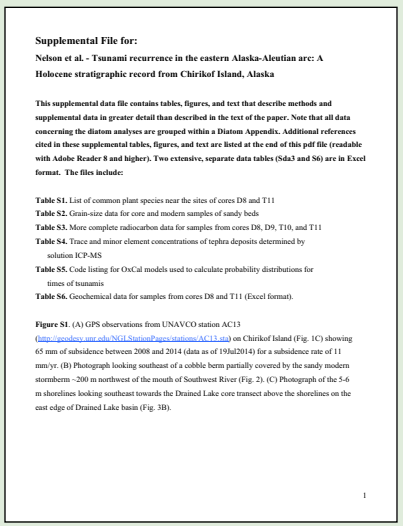

Supplemental File for:
Nelson et al. - Tsunami recurrence in the eastern Alaska-Aleutian arc: A Holocene stratigraphic record from Chirikof Island, Alaska

This supplemental data file contains tables, figures, and text that describe methods and supplemental data in greater detail than described in the text of the paper. Note that all data concerning the diatom analyses are grouped within a Diatom Appendix. Additional references cited in these supplemental tables, figures, and text are listed at the end of this pdf file (readable with Adobe Reader 8 and higher). Two extensive, separate data tables (Sda3 and S6) are in Excel format. The files include:

Table S1. List of common plant species near the sites of cores D8 and T11
Table S2. Grain-size data for core and modern samples of sandy beds
Table S3. More complete radiocarbon data for samples from cores D8, D9, T10, and T11
Table S4. Trace and minor element concentrations of tephra deposits determined by solution ICP-MS
Table S5. Code listing for OxCal models used to calculate probability distributions for times of tsunamis
Table S6. Geochemical data for samples from cores D8 and T11 (Excel format).

Figure S1. (A) GPS observations from UNAVCO station AC13 (http://geodesy.unr.edu/NGLStationPages/stations/AC13.sta) on Chirikof Island (Fig. 1C) showing 65 mm of subsidence between 2008 and 2014 (data as of 19Jul2014) for a subsidence rate of 11 mm/yr. (B) Photograph looking southeast of a cobble berm partially covered by the sandy modern stormberm ~200 m northwest of the mouth of Southwest River (Fig. 2). (C) Photograph of the 5-6 m shorelines looking southeast towards the Drained Lake core transect above the shorelines on the east edge of Drained Lake basin (Fig. 3B).

1

[1]Supplemental File. Descriptions of and quotes from four unpublished manuscripts about the history and archaeology of Chirikof Island, and an extensive Diatom Appendix with three tables of data and nine additional figures. Please visit **http://dx.doi.org/10.1130/GES01108.S1** or the full-text article on www.gsapubs.org to view the Supplemental File.

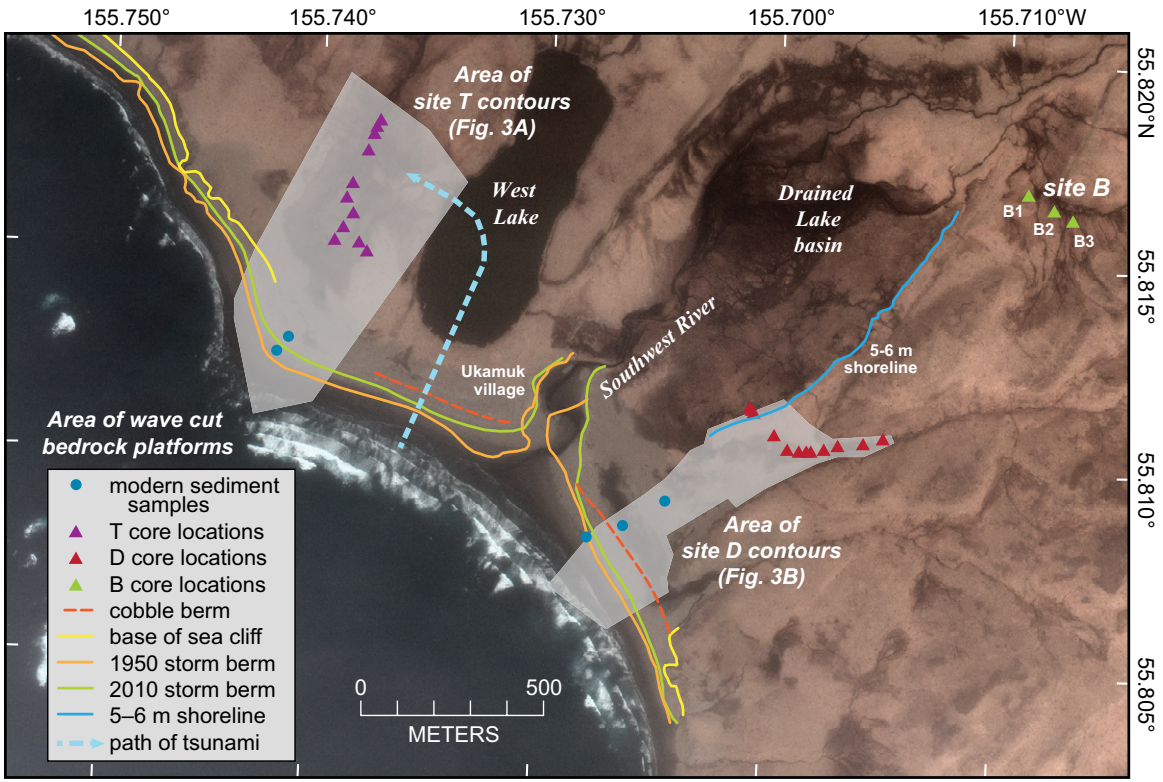

Figure 2. Locations of the Tsunami Ramp (T core locations), Drained Lake (D core locations), and Belligerent Bull (B core locations) sites and other features at Southwest Anchorage. The Southwest Anchorage place names West Lake and Southwest River follow Moore and Saltonstall and Steffian (in the Supplemental File [see footnote 1]), respectively. Approximate location of Ukamuk village, a Russian-directed hunting outpost from Saltonstall and Steffian and Clark (in the Supplemental File [see footnote 1]). Colored lines map crests of beach berms, sea cliffs, and former shorelines on the east side of the Drained Lake basin. Dashed light blue line at West Lake shows inferred path of tsunami into the Tsunami Ramp basin during deposition of bed C′ (Table 1). Blue dots show location of modern samples of beach and dune sand (Table S2 [see footnote 1]). (GeoEye-1 imagery copyright Digital Globe 2013, NextView License.)

quake. From a resident's account of tides that no longer reached as high on the west coast of the island following the 1880 earthquake as before the earthquake—and down-to-the-southeast surface displacement on a northeast-trending fault of at least 2 m (Fig. 1C)—Moore in the Supplemental File (see footnote 1) inferred southeastward tilting of the island during the earthquake. The appearance of breakers along the southwest coast of the island where none had appeared before (Lander, 1996, p. 46) also suggests uplift during the 1880 earthquake. Flat-topped ridges at 6–18 m and 40–200 m inland of the storm berm along the northwest coast are the remains of wind-eroded dunes rather than remnants of marine terraces uplifted during prehistoric earthquakes. Because there are no other reports of strong earthquake effects and a regional tsunami was not recorded, the 1880 earthquake probably occurred on an upper plate fault near Chirikof Island, possibly producing the prominent reverse-fault scarp reported in 1962 by Moore (in the Supplemental File [see footnote 1]; Davies et al., 1981; Lander, 1996; e.g., Liberty et al., 2013).

Observations at Southwest Anchorage are consistent with subsidence in the twentieth century, but rates of apparent subsidence prior to GPS observations that began in 1995 (Fournier and Freymueller, 2007) have not been accurately measured. The strongest evidence of subsidence is the inland migration of the crest of the storm-beach berm at Southwest Anchorage, which we infer was caused by relative sea-level rise during gradual subsidence. The 2010 crest is tens of meters inland of the berm crest mapped on 1952 air photographs, and the 2010 crest partially covers an older, lower berm crest composed of rounded cobbles derived from bedrock exposed in sea cliffs to the southeast (Fig. 2; Fig. S1 and Saltonstall and Steffian in the Supplemental File [see footnote 1]). Comparison of photographs of Southwest Anchorage in 1963, 2010, and 2013 shows significant erosion of the area behind the storm berm since 1963, but the distance that the berm has migrated inland is difficult to estimate from the photographs.

Comparison of 1952 air photos with recent imagery of the east coast of Chirikof Island shows tens of meters of cliff retreat and 30–60 m of westward migration of the storm berm that is consistent with island subsidence (Fig. S2 in the Supplemental File [see footnote 1]). A smooth, sandy, 100-m-wide beach on the east coast, on which twin-engine aircraft landed from the late 1940s

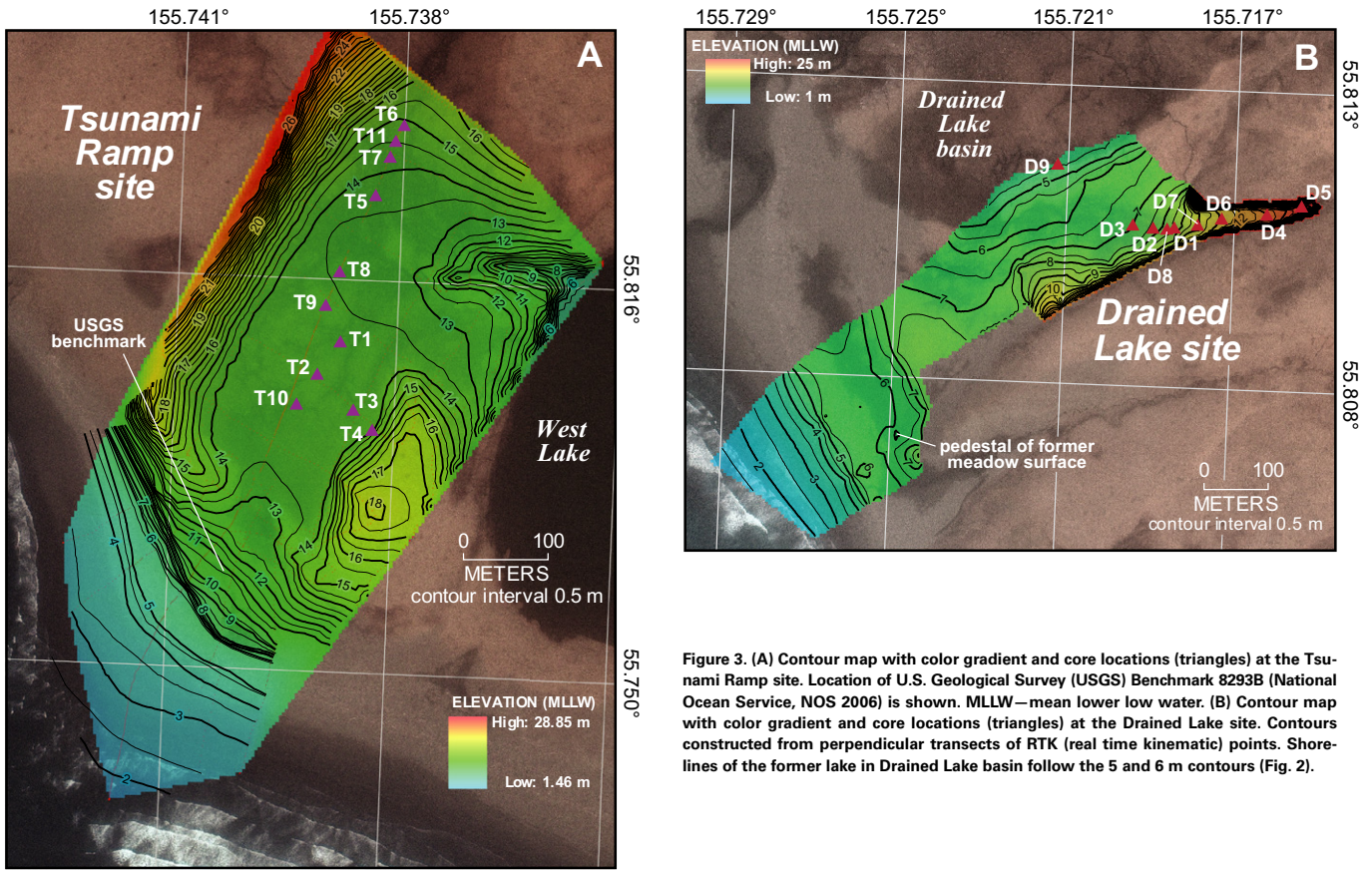

Figure 3. (A) Contour map with color gradient and core locations (triangles) at the Tsunami Ramp site. Location of U.S. Geological Survey (USGS) Benchmark 8293B (National Ocean Service, NOS 2006) is shown. MLLW—mean lower low water. (B) Contour map with color gradient and core locations (triangles) at the Drained Lake site. Contours constructed from perpendicular transects of RTK (real time kinematic) points. Shorelines of the former lake in Drained Lake basin follow the 5 and 6 m contours (Fig. 2).

into the 1970s (Keithahn, 1962; Long, 1975; Chaffin et al., 1983; Fields, 2000; Saltonstall and Steffian in the Supplemental File [see footnote 1]), is now less than a few tens of meters wide and is rocky and covered with debris. Perhaps an increased intensity of storms, higher wave heights, or changes in marine currents aided cliff retreat and landward migration of storm berms (e.g., Allan and Komar, 2006), but we doubt if only hydrographic factors can fully account for such shoreline changes.

Primary Study Sites

Our primary study sites are two small valleys at Southwest Anchorage (Figs. 2 and 3). Key selection criteria were that the sites be high enough (7–15 m) and/or far enough inland (500–700 m) to exclude deposition of sand during storm surges, and low enough that they would be inundated by high tsunamis traveling inland from the beach. Although we have no storm-surge or wave-height measurements from Chirikof Island, we infer that both sites are too high and too far inland for storm waves to have deposited sand beds at the sites with sea level near its present position (discussed in the following). We also chose sites underlain by at least 4 m of freshwater peat in which sand beds deposited by tsunamis should be distinct.

Our Tsunami Ramp site is a 100 m by 500 m gently sloping basin covered with muskeg and bog vegetation (list of common plant species in Table S1 in the Supplemental File [see footnote 1]). Low dunes front the south lip of the basin at 13 m elevation ~180 m inland from the modern storm berm. No streams enter the basin, which has a drainage area of <0.4 km^2. More than two-thirds of the Tsunami Ramp basin drains into adjacent West Lake through a small stream near the basin's northeast corner.

Our Drained Lake site is a 150-m-long alluvial fan covered with muskeg vegetation that gently slopes from 5 to 15 m between the mouth of a <10-m-wide stream valley and the shorelines on the southeast edge of Drained Lake basin ~550 m inland from the ocean beach (list of common plant species in Table S1 in the Supplemental File [see footnote 1]). The drainage basin is small (<0.4 km^2) and the steep sides (30°–40°) of the V-shaped stream valley are well stabilized by vegetation.

Reconnaissance Sites

We also briefly explored stratigraphy at two reconnaissance sites: (1) the Belligerent Bull site ~1.5 km inland in the valley of Drained Lake basin (site B, Fig. 2), and (2) in a 600-m-long, southwest-facing valley, the site of the most recently occupied cattle ranch on the island called New Ranch (Fields, 2000; Fig. 1B). The Belligerent Bull site consists of the distal parts of gently sloping fans (7–10 m elevation), covered with muskeg vegetation like that at the Drained Lake site, on either side of a small intermittent stream that flows into the Drained Lake basin. At New Ranch valley, ~2.3 km south of the Drained Lake site (Fig. 1C), a stream meanders across the 250-m-wide valley floor of marshy meadows at ~6–10 m elevation. A sandy, cobbly storm berm, 2–4 m high with 2–3-m-high dunes behind it, protects the valley from all but the highest storm waves.

IDENTIFYING TSUNAMI DEPOSITS

Following many studies of Holocene tsunami deposits (e.g., Smith et al., 1983; Minoura and Nakata, 1994; Nanayama et al., 2003; Witter et al., 2009; Chagué-Goff et al., 2012; Sawai et al., 2012), we explored the Tsunami Ramp (site T) and Drained Lake (site D) sites for potential tsunami deposits (potential deposits consist of probable and possible deposits, as discussed in the following) with handheld gouge (25 mm diameter) and Russian (50 mm diameter) corers (methods reviewed by Nelson, 2015; Fig. 3). A few reconnaissance cores were described 1 km northeast (Belligerent Bull site) and 2.4 km south (New Ranch valley) of the Drained Lake site (Figs. 1B and 2). The small valleys that we cored lacked exposures and high water tables in valley sequences of freshwater peat precluded hand-dug pits. The wettest, windiest August weather in decades prevented more detailed sampling and investigation of more widely distributed sites.

General descriptions of cores were made in the field (Tables 1 and 2); detailed lithologic descriptions of cores returned to the laboratory followed the system of Tröels-Smith (1955; e.g., Nelson, 2015). Macroscopic laboratory descriptions were confirmed through examination of 74 smear slides, grain-size analysis of 58 samples of sandy beds (Table S2 in the Supplemental File [see footnote 1]), and CT (three-dimensional computer tomography) X-ray scans (methods of Rothwell and Rack, 2006; Davies et al., 2011) of selected segments of cores T11 and D8. We used these data to correlate sandy and silty lithofacies in transects of cores along the axes of the Tsunami Ramp and Drained Lake sites (Figs. 4 and 5) and dated many of the beds with 37 radiocarbon ages (Table 3; Table S3 in the Supplemental File [see footnote 1]).

The characteristics of modern and Holocene tsunami deposits have been extensively reviewed (e.g., Dawson et al., 1991; Minoura and Nakaya, 1991; Hemphill-Haley, 1996; Dawson and Shi, 2000; Dominey-Howes et al., 2006; Morton et al., 2007; Shiki et al., 2008; Bourgeois, 2009; Apotsos et al., 2011; Szczuciński et al., 2012). Although some characteristics are common to many tsunami deposits, most deposit characteristics are strongly dependent on site geomorphology and sediment sources. Distinguishing between sand beds deposited landward of the shore during the largest storms and by tsunamis can be problematic at some sites, although general discriminating criteria were proposed (Nanyama et al., 2000; Witter et al., 2001; Goff et al., 2004; Tuttle et al., 2004; Kortekaas and Dawson, 2007; Morton et al., 2007; Switzer and Jones, 2008). Multiple lithologic, stratigraphic, and site geomorphic criteria, commonly supported by paleontological, geochemical, anthropological, or historical analog data, are required to show deposition by a tsunami (Peters and Jaffe, 2010; Goff et al., 2010; Szczuciński et al., 2012; Chagué-Goff et al., 2015).

We use the following field-based lithologic and stratigraphic characteristics to infer a tsunami or non-tsunami genesis for potential tsunami deposits: lithology; degree of sorting; internal structures, such as fining-upward beds, multiple laminae, or clasts of mud or peat; sharpness of contacts; uniformity in bed thickness; and lateral and elevational extent of beds. Relying primarily on these field-based criteria, we describe the characteristics of each silty to sandy lithofacies (bed) at each site and then infer a (1) probable tsunami, (2) possible tsunami, or (3) non-tsunami genesis for each bed, as shown in Tables 1 and 2. All beds from both sites are labeled with consecutive letters in sequence from youngest to oldest (A to *e′*, Tables 1 and 2; Figs. 4 and 5). Uppercase letters indicate probable tsunami beds; lowercase letters indicate possible tsunami beds. Labels for beds that we do not interpret as possible tsunami deposits are in lowercase italics. We then compare our inferences about bed genesis based on stratigraphic and grain-size data with diatom assemblage and geochemical data for lithofacies from one core at each site to determine the extent to which the diatom and geochemical data confirm a marine source for potential (probable and possible) tsunami deposits (Figs. 4–8; Table S2 in the Supplemental File [see footnote 1]). We defer discussion of possible alternative processes of deposition until after our summary of the evidence.

Lithofacies Description and Genesis

Tsunami Ramp Site

Lithofacies exposed in 10 cores along the axis of the Tsunami Ramp basin (site T) consist of thin beds of sandy or silty sediment within a sequence of 3–5 m of freshwater peat (Figs. 3A and 4). Probable and possible correlations of these beds show that only five beds extend across much of the long axis

TABLE 1. CHARACTERISTICS OF CORRELATED SANDY OR SILTY BEDS IN CORES FROM THE TSUNAMI RAMP SITE (SITE T)

Bed label and genesis[1]	Correlative depth in core T11 (cm)	Identified in core (T) numbers	Range in lithology[2]	Mean grain-size distribution[3]	Thickness range (mean ± standard deviation)[4] (mm)	Lateral extent[5] (m)	Elevation reached (m)	Distinctness of bed (number of laminae)[6]	Upward grading	Sharpness of contacts upper/lower[7] (mm)	Comments
j	75	11, 6	slightly sandy peat	—	2–70	25	13.8	less distinct		5/5	Sandy peat lithology suggests that this bed does not correlate with a distinct gray silty bed at 12.9 m elevation in core T2.
v	118	5, 6, 11, 1, 8	silty peat to sandy peat to sand	—	5–21	279	13.5	indistinct		2/3	
W	123	10, 1, 8, 5, 7, 11, 6	silty peat to silt over sand	4.21	3–20 (8 ± 5)	375	13.5	indistinct (2)	normal	1/1*	Two 1– 2-mm-thick laminae; correlation to core T10 uncertain because bed v is not present in core T10.
X	128	5, 7, 11, 1	clean sand over slightly silty sand to silty peat	3.91	8–22 (15 ± 5)	254	13.4	indistinct (2)	inverse	2/2	
Y	133	10, 3, 2, 1, 9, 8, 5, 7, 11, 6	clean sand	3.57–3.80 (2)	5–30 (14 ± 6)	375	13.4	distinct (2)	normal	2/1*	Several characteristics typical of tsunami deposits, such as silt rip-up clasts in clean sand, distinct laminae, and normal upward grading.
z	170	9, 6, 11, 1	slightly silty peat to peaty silt	—	20–40 (30 ± 7)	235	12.7	indistinct		6/1	Light colored bed; 5YR color suggests silt may be reworked from tephra 1 or a similar tephra.
a′	176	8, 9, 6, 11, 1, 10	slightly silty peat to slightly peaty silt	—	3–20 (12 ± 6)	375	12.7	indistinct		2/2	Light colored bed; 5YR color suggests silt may be reworked from tephra 1 or a similar tephra.
b′	192	1, 8, 9, 10	slightly silty peat to peaty sandy silt	—	3–41 (20 ± 12)	183	12.5	less distinct		2/1	Light colored bed with more distinct contacts than beds *z* and *a′*; 5YR color suggests silt may be reworked from tephra 1 or a similar tephra.
C′	224	10, 3, 2, 1, 9, 8, 5, 7, 11, 6	sandy silt over sand	4.25–6.11 (38)	25–220 (106 ± 52)	375	12.5	distinct (2)	normal	3/1*	The thickest and most distinct tsunami deposit found; pronounced upward grading from fine sand to silt (Fig. 7).
d′	265	5, 7, 6, 11, 8	silty peat to sand to silt	—	2–40 (11 ± 14)	192	12.1	distinct		3/1*	Light gray color and silty to sandy lithology suggest deposition in quiet water.
e′	293	10, 1, 5, 6, 7, 8, 11	silty sand to clayey silt		3–110 (33 ± 38)	200?		distinct (2)		2/0.5*	Early postglacial(?) pond deposits derived from silty diamicton; 2 mm clayey silt laminae present in some cores; 3–5-cm-thick peaty silt beds in others.

[1]Bed labels are consecutive letters from youngest to oldest at both the Tsunami Ramp and Drained Lake sites. Uppercase letters label beds having distributions and characteristics that strongly suggest deposition by a tsunami; lowercase letters show possible tsunami deposits. Labels for beds that we do not interpret as tsunami deposits are shown in lowercase italics. Beds identified in only one core (beds in T4, T2, and just above bed C′ in T10, Fig. 4) are not listed. We examined smear slides of all beds and diatom samples from all beds except bed v.

[2]Range in dominant lithology of bed in correlated cores. In most beds sand size is very fine sand, ranging to fine sand for beds W, X, and in the lower part of bed C′.

[3]Range in Folk and Ward (1957) mean grain-size (phi units) for analyzed samples (number of samples in parentheses). Dash indicates that no samples were analyzed from this bed.

[4]Mean thickness and one standard deviation for beds in three or more cores. Large standard deviations show large variability in thickness for most beds.

[5]Distance between most widely spaced cores in which bed is identified.

[6]Distinctness based on sharpness of contacts, contrast in lithology with underlying and overlying peat, and contrast in Munsell color hues and values. Number of internal laminae in bed (in parentheses) as observed in the field, in photographs, or in three-dimensional X-ray scans of core T11.

[7]Average of measurements on the most distinct beds (sharpest contacts), mostly from photographs (*indicates lower contact sharpness of 0.5 mm in at least one core).

of the basin. Slight downcore differences in peat color and density, some of which are correlative among 2–5 cores, suggest periods of relative dryness, but no well-developed soil horizons were identified. CT X-ray scans (e.g., Fig. S3 in the Supplemental File [see footnote 1]) show that peat density increases gradually with depth, consistent with autocompaction of the peat (e.g., Brain et al., 2011).

We found only two field-identifiable tephra beds in the Holocene sequence at the Tsunami Ramp site, identified by their pale tan and orange colors and abundance of elongate, angular glass and mineral silt grains (tephra beds 1 and 2; Figs. 4 and 6; Fig. S3 in the Supplemental File [see footnote 1]). We used the tephra beds only for stratigraphic correlation of Tsunami Ramp cores with cores at the Belligerent Bull site (Fig. 2; Fig. S3 in the Supplemental File [see footnote 1]); we did not use them for dating. Geochemical analyses of tephra silt fractions (Table S4; Fig. S4 in the Supplemental File [see footnote 1]) and possible correlations of tephra beds 1 and 2 with other Aleutian tephra are discussed in the Supplemental File (see footnote 1).

TABLE 2. CHARACTERISTICS OF CORRELATED SANDY OR SILTY BEDS IN CORES FROM THE DRAINED LAKE SITE (SITE D)

Bed label and genesis[1]	Depth in core D8 (cm)	Identified in core D numbers	Range in lithology[2]	Mean grain-size distribution[3]	Thickness range (mean ± standard deviation)[4] (mm)	Lateral extent[5] (m)	Elevation reached (m)	Distinctness of bed[6] (number of laminae)	Upward grading	Sharpness of contacts upper/lower[7] (mm)	Comments
A	14	3, 2, 8, 1, 7	clean sand to slightly silty sand	2.23–2.36 (3)	4–44 (27 ± 11)	100	9.8	distinct		2/1	Mixed with upper and lower peat in core D1.
b	17	3, 2, 8, 1	slightly silty sand to sand	—	5–16 (12 ± 5)	55	8.3	less distinct		2/2	Greater mixing of sand with upper and lower peat than in bed A.
C	28	3, 2, 8, 1, 7	clean sand to peaty sand	—	8–18 (14 ± 4)	100	9.6	distinct		2/2	Mixed with upper and lower peat in cores D3 and D7.
D	43	3, 2, 8, 1, 7, 6, 4, 5	clean sand to sandy silt over sand	—	8–33 (16 ± 8)	265	14.8	distinct	normal	1/1	Thickness including overlying sandy silt in highest core D5 is 65 mm.
E	52	2, 8, 1, 7	slightly silty sand to peaty sand	—	8–25 (16 ± 9)	70	9.4	indistinct		4/3	More distinct near base of section of peaty sand; may correlate with similar bed in similar stratigraphic position in core D5.
f	79	8, 2	sand to peaty sand to sandy peat	—	8–25 (18 ± 9)	21	7.5	distinct (2)		8/6	Distinct sand bed in cores D8 and D2; may correlate with similar bed in similar stratigraphic position in core D5.
g	120	2, 8, 7, 6	sand to peaty sand	—	3–135 (43 ± 62)	106	9.9	distinct		2/1	Bed within thick section of peaty sand; less distinct in core D6; may correlate with similar bed in similar stratigraphic position in highest core D5.
H	175	3, 2, 8, 7, 6, 4, 5	clean sand to silty sand	1.98–2.23 (3)	5–40 (22 ± 13)	265	13.7	distinct	inverse, normal	2/2	Distinct in all listed cores.
I	208	3, 2, 8, 1, 7, 6, 4, 5	clean sand to peaty sand	—	8–110 (34 ± 37)	265	13.2	distinct		2/2	Distinct in all listed cores.
K	220	8, 1, 7, 6	clean sand to peaty sand to silty peat	—	4–28 (11 ± 12)	85	8.5	distinct		2/1	Within section of silty peat in core D8.
l	273 (core 7)	6, 7	silty sand	—	14–50	34	—	distinct		3/2	Bed sharply overlies fibrous peat in both cores; silt and clasts in sand suggest fluvial origin.
m	260	3, 2, 8	sand and peaty sand	—	5–20	51	5.6	less distinct (3)		2/1	5-mm-thick laminae of slightly deformed clean sand; deformation possibly due to melting of snow beneath bed of wind-blown sand deposited in winter.
N	290	3, 2, 8, 1, 7, 6, 5?	clean sand to sandy silt to gravelly sandy diamicton	0.87	25–147 (67 ± 42)	265	12.8	distinct	normal	2/1	Correlation of clean sand with peaty sandy silt or gravelly sandy diamicton in cores D7 and D6 suggests it is contemporaneous with a debris-flow deposit in higher cores.
O	296	3, 8, 1, 7	clean sand to peaty sand	—	3–78 (25 ± 31)	100	6.4	distinct (2)		1/1	Two 5-mm-thick clean sand laminae in sandy peat section in core D8; may correlate with similar bed in similar stratigraphic position in highest core D5.
P	312	3, 2, 8, 1, 7	clean sand to peaty sand	—	8–102 (34 ± 35)	100	6.0	distinct		2/2	One thick sand bed in one segment and two thinner sand beds in a second overlapping segment of core D8; may correlate with similar bed in similar stratigraphic position in core D5.
Q	322	3, 2, 8, 1, 7	clean sand to peaty sand	—	7–69 (42 ± 25)	100	6.0	distinct (2)	normal	3/1	Upper 10 mm of bed fines upward; peat clasts in sand in core D8.
R	351	3, 2, 8, 1, 7, 6	clean sand	2.24–4.03 (6)	3–64 (40 ± 21)	136	6.6	distinct	normal	2/1	
S	356	8, 1, 7, 6	clean sand	1.55–2.22 (3)	18–55 (35 ± 19)	85	6.5	distinct	normal	2/1	Similar to bed R.
t	370	2, 8	clean sand to peaty sand	—	12–90	21	4.5	distinct		2/2	Similar to beds P and Q; not inferred to be probable tsunami deposit because it is found in only two cores.
u	381	8, 1, 6	clean sand to peaty sand	—	8–65 (27 ± 24)	85	6.3	distinct		1/3	Similar to beds P and Q; not inferred to be probable tsunami deposit because it is found in only three cores.

[1]Bed labels are consecutive letters from youngest to oldest at both the Tsunami Ramp and Drained Lake sites. Uppercase letters label beds having distributions and characteristics that strongly suggest deposition by a tsunami; lowercase letters show possible tsunami deposits. Label for bed *l*, which we do not interpret as a tsunami deposit, is shown in lowercase italics. Beds identified in only one core (at least 12 beds in core D5, and 1–3 beds in D6, D7, and D2) are not listed. We examined smear slides from listed beds and diatom samples from all beds except *l* and m.

[2]Range in lithology of beds in correlated cores. Sand size is fine to very fine sand, with more fine sand and minor medium sand in better sorted beds.

[3]Range in Folk and Ward (1957) mean grain-size (phi units) for analyzed samples (number of samples in parentheses). Dash indicates that no samples were analyzed from this bed.

[4]Mean thickness and one standard deviation for beds in three or more cores. Large standard deviations show large variability in thickness for most beds.

[5]Distance between most widely spaced cores in which bed is identified.

[6]Distinctness of bed based on sharpness of contacts, contrast in lithology with underlying and overlying peat, and contrast in Munsell color hues and values. Number of internal laminae in bed (in parentheses) as observed in the field, in photographs, or in three-dimensional X-ray scans of core D8.

[7]Average of measurements on the most distinct beds (sharpest contacts), mostly from photographs (*indicates lower contact sharpness of 0.5 mm in at least one core).

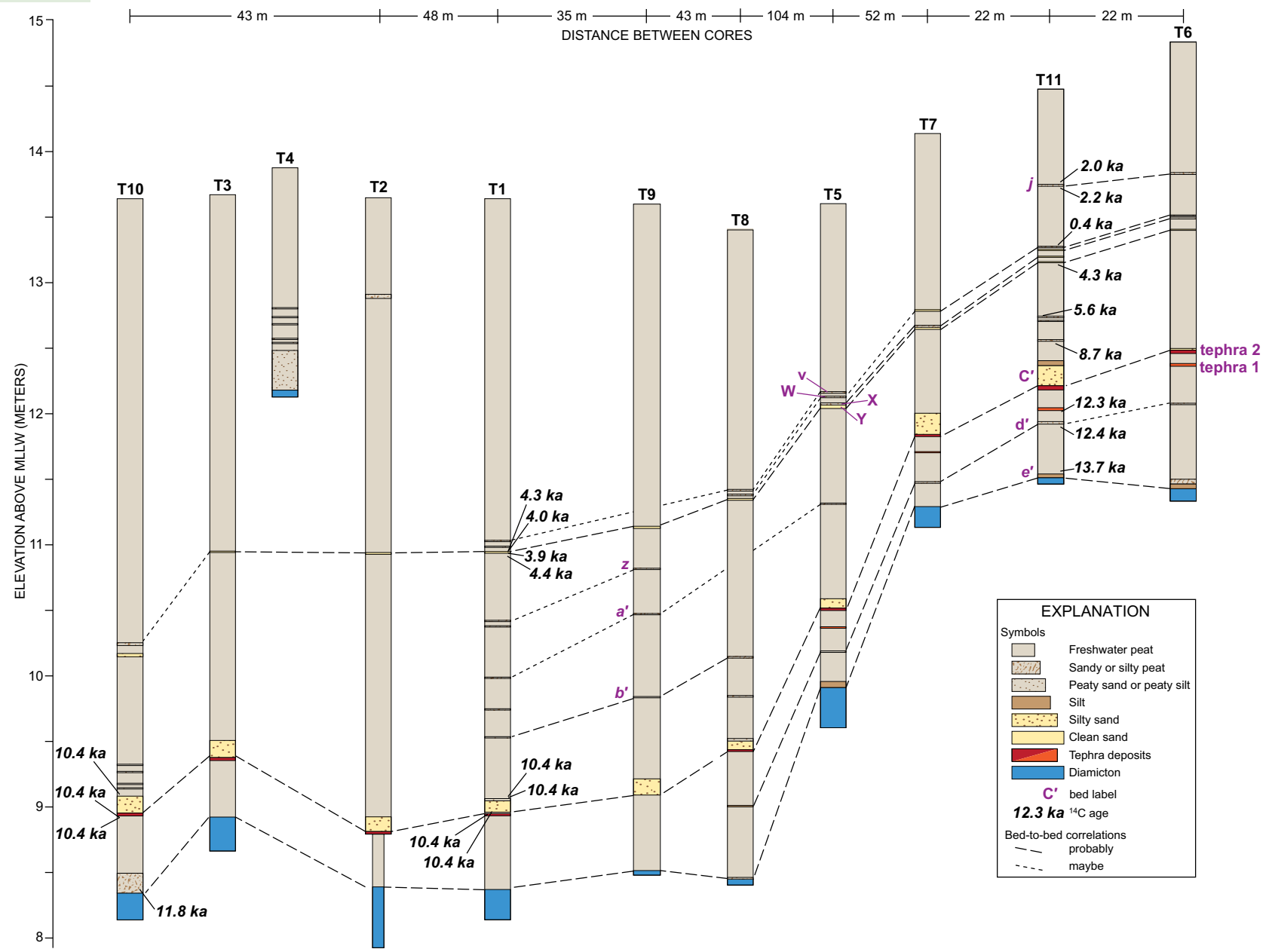

Figure 4. Correlation of 10 axial cores at the Tsunami Ramp site. Core T4, off the axis of the basin on its southeast flank (Fig. 3A), reached till at a shallow depth. Russian cores (5 cm diameter; wide columns in figure) and gouge cores (2.5 cm diameter; narrow column at base of core T2) were described and photographed in the field. Cores T1, T11, and the lower part of core T10 were described and sampled in detail in the laboratory. Bed labels as in Table 1. Accelerator mass spectrometer ^{14}C ages are the mode of the calibrated probability age distribution rounded to the nearest century (Table 3). MLLW—mean lower low water.

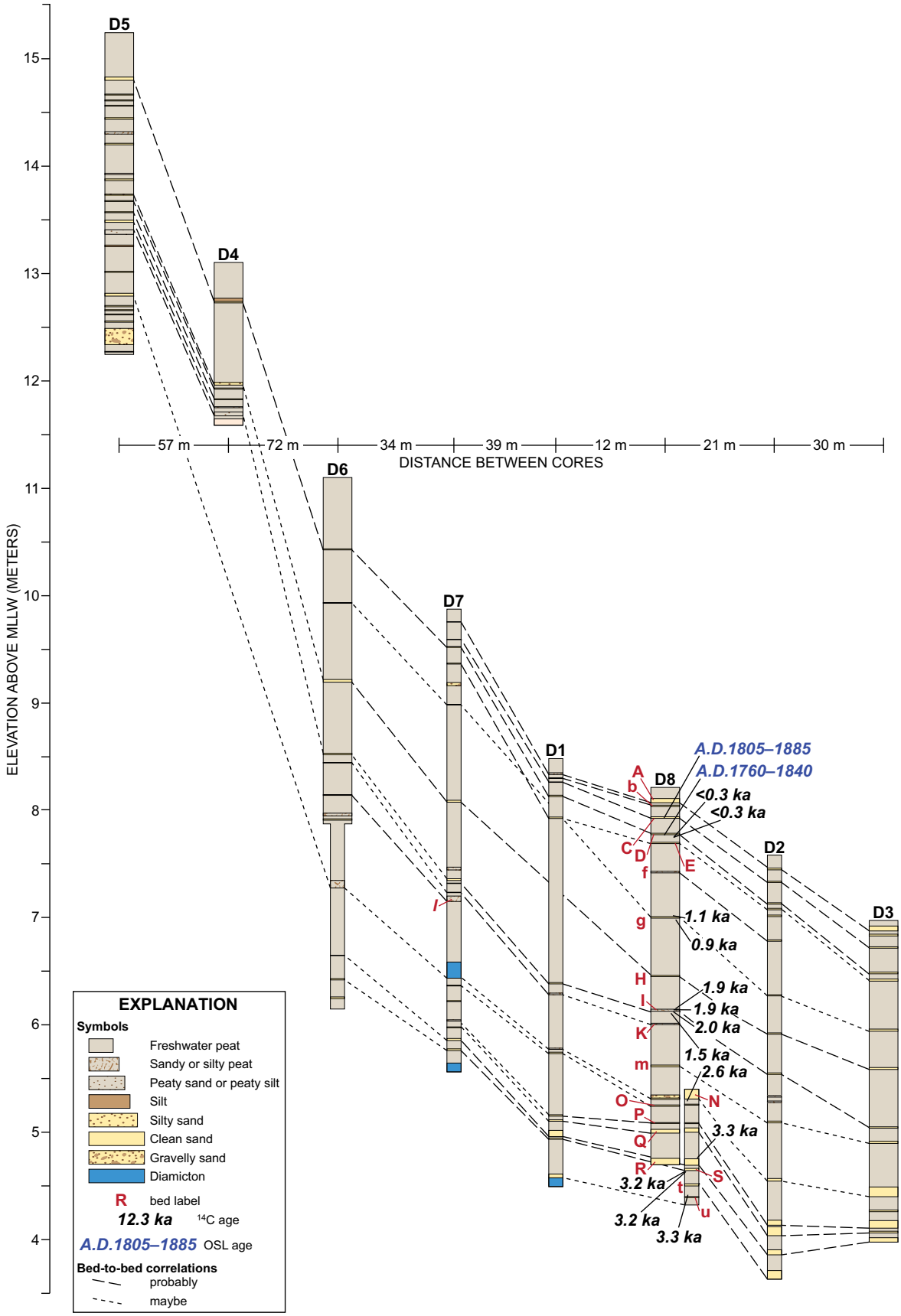

Figure 5. Correlation of axial cores at the Drained Lake site. Gouge cores (2.5 cm diameter; narrow columns) and Russian cores (5 cm diameter; wide columns) were described and photographed in the field. Core D8 was described and sampled in detail in the laboratory. Bed labels as in Table 2. Accelerator mass spectrometer ^{14}C ages are the mode of the calibrated probability age distribution rounded to the nearest century (Table 3). Data for optically stimulated luminescence (OSL) ages are in Table 4. MLLW—mean lower low water.

TABLE 3. SUMMARY OF ^{14}C DATA FOR SAMPLES FROM FRESHWATER PEAT IN CORES D8, D9, T1, T10, AND T11

Core and OxCal bed age[1]	Bed label[2]	Calibrated age[3] (cal yr B.P.; 2σ)	Laboratory reported age[4] (^{14}C yr B.P.)	Provenance interpretation[5]	Depth in core[6] (cm)	Description of dated material[7]
Core T1						
4360–4105	Y	4408–4153	**3845 ± 35**	**minimum?**	268–268.5	9 charcoal(?) spheres and 1 beetle carapace from peat above sand.
	Y	4153–3930	3710 ± 35	minimum?	268–268.5	Abraded 2-mm-diameter woody root or twig from peat above sand.
	Y	3983–3836	3605 ± 30	minimum	270–270.5	Black 3-mm-diameter herb rhizome at base of sand.
	Y	4525–4244	3950 ± 50	maximum	270.5–272	15 charcoal(?) spheres and 1 beetle carapace from peat beneath sand.
10,518–10,284	C′	10,586–10,277	9280 ± 50	minimum	454–456.5	12 identified herb seeds from peat above silty sand.
	C′	10,586–10,297	**9290 ± 40**	**minimum**	454–456.5	56 *Potamogeton* sp. seeds from peat above silty sand.
	C′	10,515–10,248	**9220 ± 50**	**maximum**	468	Fragment of deciduous leaf, horizontal at lower contact of silty sand.
	C′	10,581–10,292	9280 ± 45	maximum	467–469	~150 *Sphagnum* sp. stems from peat beneath silty sand.
Core T10						
	C′	10,501–10,275	9230 ± 30	minimum	468.5–469	Herb rhizome from peat above silty sand.
(bed is 1 cm	C′	10,658–10,219	9220 ± 100	maximum	479–479.5	14 *Sphagnum* sp. stems from peat beneath tephra 2.
above tephra 2)	C′	10,505–10,279	9235 ± 30	maximum	479–479.5	4 woody twigs with leaf scars from peat beneath tephra 2.
	e′	12,044–11,630	10170 ± 45	minimum	525–527	~80 fragments of *Sphagnum* sp. stems from peat above till.
Core T11						
2115–1906	*j*	2106–1898	**2030 ± 30**	**minimum?**	67–70	3 oval yellow seed halves from peat above sandy peat.
	j	2315–2115	**2180 ± 30**	**maximum**	76–78	Abraded fragment of herb stem from peat beneath sandy peat.
	W	510–317	385 ± 35	minimum	120–122	12 *Sphagnum* sp. stems (submodern) and 2 beetle backs from peat above thin sand.
4360–4105	Y	4415–4160	**3870 ± 30**	**maximum?**	133–135	2 fragments of decayed, woody root from peat beneath peaty sand.
5640–5000	*z*	5658–5471	**4840 ± 45**	**maximum**	165–167	3 insect parts, 3 fragments of woody roots from peat above silty peat.
8741–7280	*b*′	8856–8455	**7830 ± 50**	**maximum**	193–196	1 seed and 6 yellow seed halves from peat below silty peat.
12,405–11,469	tephra 1	12,525–12,068	**10400 ± 55**	**maximum?**	244.2–246	Decayed ring structures from herb rhizome from peat below tephra 1.
13,669–12,966	d′	13,388–11,411	**10,750 ± 360**	**maximum**	267–270	One-half of yellow seed from peat below silty peat.
13,925–13,483	*e*′	13,957–13,476	**11,900 ± 90**	**minimum?**	286–289	2 smooth woody stems from peat above silt.

(*continued*)

TABLE 3. SUMMARY OF ^{14}C DATA FOR SAMPLES FROM FRESHWATER PEAT IN CORES D8, D9, T1, T10, AND T11 (*continued*)

Core and OxCal bed age[1]	Bed label[2]	Calibrated age[3] (cal yr B.P.; 2σ)	Laboratory reported age[4] (^{14}C yr B.P.)	Provenance interpretation[5]	Depth in core[6] (cm)	Description of dated material[7]
Core D8						
206–131	D	286–0	160 ± 30	minimum	43.5–45	2 herb stem bases connected to rhizome from peat below clean sand.
	D	305–0	210 ± 30	maximum?	43.5–45	4-mm-diameter abraded woody root or twig from peat below clean sand.
1171–977	g	1173–981	**1160 ± 30**	**minimum**	116–118	Herb rhizome with stem bases attached from peat above peaty sand.
	g	965–794	990 ± 40	max or min	121–123	Rhizome, beetle carapace, and seed case from peat below sandy peat.
2008–1833	I	1566–1353	1580 ± 50	minimum	209–211	6-mm-diameter ringed herb rhizome from peat below sandy peat.
	I	1986–1825	1950 ± 30	minimum?	205–207	2-mm-diameter unabraded, smooth, root from peat above sandy peat.
	I	2044–1743	**1960 ± 50**	**minimum**	205–207	5 *Scirpus* sp. seeds from peat above sandy peat.
	I	2115–1949	**2060 ± 25**	**maximum**	209–211	2-mm-diameter smooth herb stem from peat below sandy peat.
2707–2385	O	2739–2492	**2520 ± 25**	**maximum?**	296–298	Fragments of coarse bark from twig or root from peat below sandy peat.
3176–2891	R	3355–3162	3040 ± 30	maximum	343–344	4-mm-diameter, unabraded, woody twig from peat above clean sand.
3243–2990	S	3320–3071	**2985 ± 30**	**maximum?**	356–358	3-mm-diameter woody twig or root from peat below clean sand.
	S	3320–3075	2990 ± 30	maximum?	356–358	Casing of black herb rhizome from peat below clean sand.
3547–3372	u	3479–3367	**3210 ± 30**	**minimum**	378–380	Dark brown herb rhizome from peat above lowest sand.
	u	3554–3079	3120 ± 80	max or min	378–380	1 *Scirpus* sp. seed, 2 seed casings, 1 beetle from peat above lowest sand.
Core D9						
	--	3627–3448	3300 ± 35	maximum	93–95	11 oval seeds with large top pore from lowest peaty bed in core.
	--	3980–3730	3580 ± 35	maximum	92–95	1 *Potamogeton* sp. seed and 4 yellow oval seeds from lowest peaty bed.

[1]Core number and OxCal age intervals (cal yr B.P. at 2σ) only for beds whose age is modeled using ages in bold in column labeled Laboratory reported age. The OxCal age model (V-sequence analysis feature of OxCal, version 4.2; Bronk Ramsey, 2008, 2009; probability method; e.g., Kelsey et al., 2005; Goldfinger et al., 2012) uses minimum and maximum ages for sandy beds, as noted in column labeled Provenance interpretation, and assumes constant peat deposition rates (with 25% errors) between ^{14}C-dated beds. Age intervals for non-^{14}C -dated beds in Figure 11 were calculated using bed depths and the assumed rates of peat deposition.

[2]Bed labels for potential tsunamis deposits (see Tables 1 and 2). Dated bed near base of core D9 not labeled.

[3]Calibrated ages in solar years calculated using OxCal (version 4.2; Bronk Ramsey, 2009; probability method) with the INTCAL13 atmospheric dataset (Reimer et al., 2013). Ages show time intervals of >95% probability distribution at 2σ (cal yr B.P.).

[4]Ages reported by radiocarbon laboratory (laboratory numbers in Table S3 [see footnote 1]). Quoted errors for ages are the larger of counting error or target reproducibility error. Ages for each bed selected for the OxCal model (in bold) are the oldest minimum age and the youngest maximum age for samples whose stratigraphic context in column labeled Provenance interpretation is unambiguous.

[5]Interpretation of the provenance, or stratigraphic context, of the dated sample relative to the time that host peat was deposited. Maximum ages are on samples containing carbon judged to be older than a sandy bed; minimum ages are on samples judged younger than a sandy bed.

[6]Sample picked from peat at depth or depth interval in the core shown in this column.

[7]Description and stratigraphic context (relative to sandy bed) of submitted sample material picked from peat in Russian cores or gouge cores (Figs. 4, 5, and 9). Selection and preparation methods as described by Kemp et al. (2013).

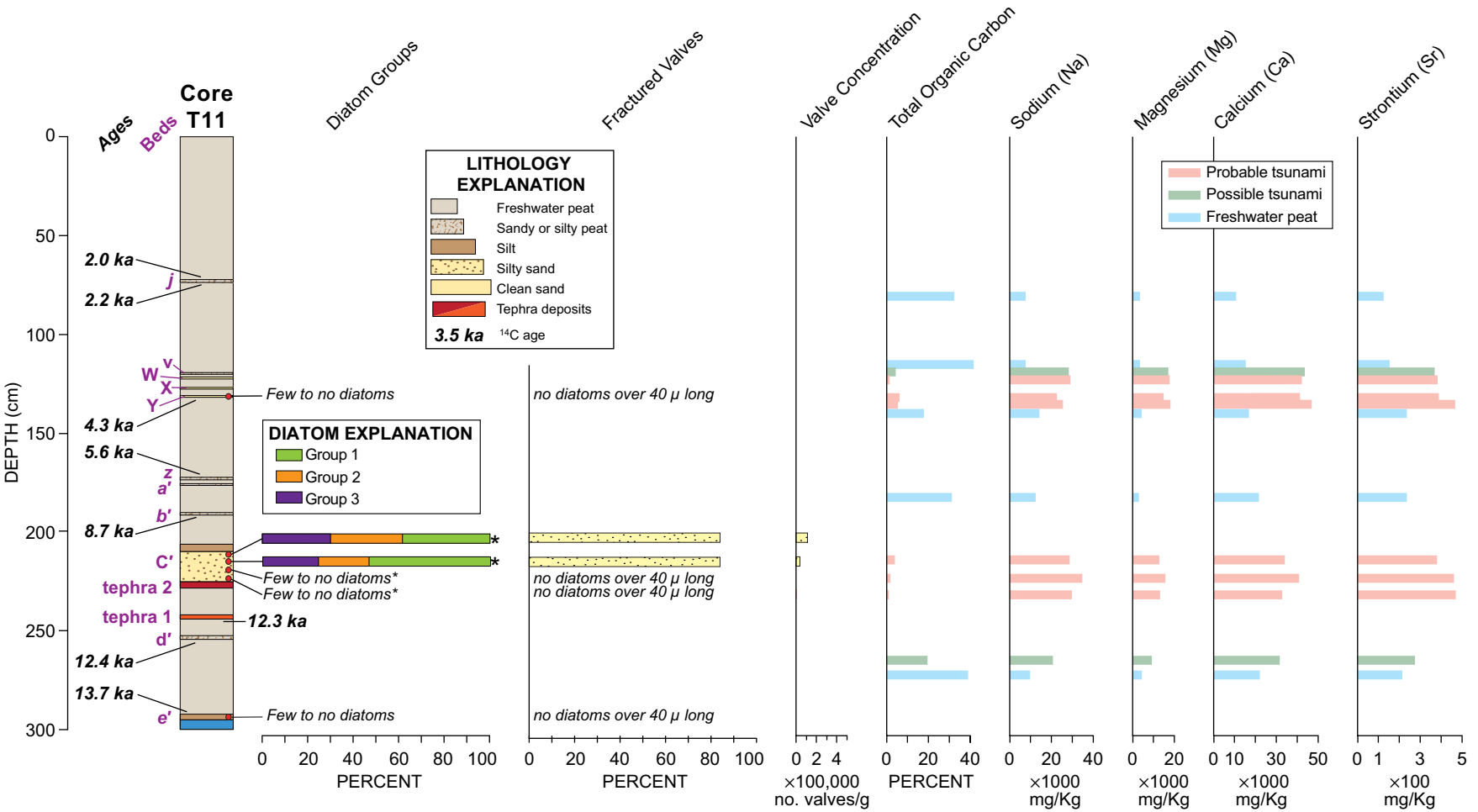

Figure 6. Core T11 at the Tsunami Ramp site showing lithology, key accelerator mass spectrometer ¹⁴C ages (Table 3), and selected diatom and geochemical data for samples from the core (complete data in Supplemental File [see footnote 1]). Bed labels as in Table 1. Asterisks mark diatom samples from core T1 shown in the equivalent stratigraphic position on core T11. Diatoms are grouped according to their preferred habitat. Group 1—benthic diatoms commonly found in acidic, freshwater peat bogs (e.g., Rühland et al., 2000). Group 2—four species of *Aulacoseira*, a freshwater planktonic genus commonly found within freshwater peat diatom flora (Crawford et al., 2003). Group 3—small, tychoplanktonic alkaliphilous taxa commonly found in shallow freshwater environments (Brugam and Swain, 2000; Tingstad et al., 2011). Colors of bars showing geochemical analyses on the right indicate samples from probable and possible tsunami deposits (Table 1) and peat.

Bed C′ is the most widespread and has the most distinct characteristics typical of tsunami deposits of any of the sandy to silty lithofacies studied (Table 1; Figs. 4 and 6; Fig. S3 in the Supplemental File [see footnote 1]). The bed rises landward from 9 m to 12.5 m, is thicker than other sandy and/or silty beds in the 10 axial cores, consistently fines upward from silty very fine sand to silt (Fig. 7; Table S2 in the Supplemental File [see footnote 1]), and has very sharp (0.5–1 mm thick), planar to irregular lower contacts in all cores, suggesting erosion of underlying peat or tephra. The massive structure and consistent upward grading of this 55–220-mm-thick bed indicate suspension deposition from water with high concentrations of coarse and medium silt. Smear slides from bed C′ show an abundance of silt-sized angular glass and mineral grains reworked from underlying tephra 2 (Fig. Sda9 in the Supplemental File [see footnote 1]).

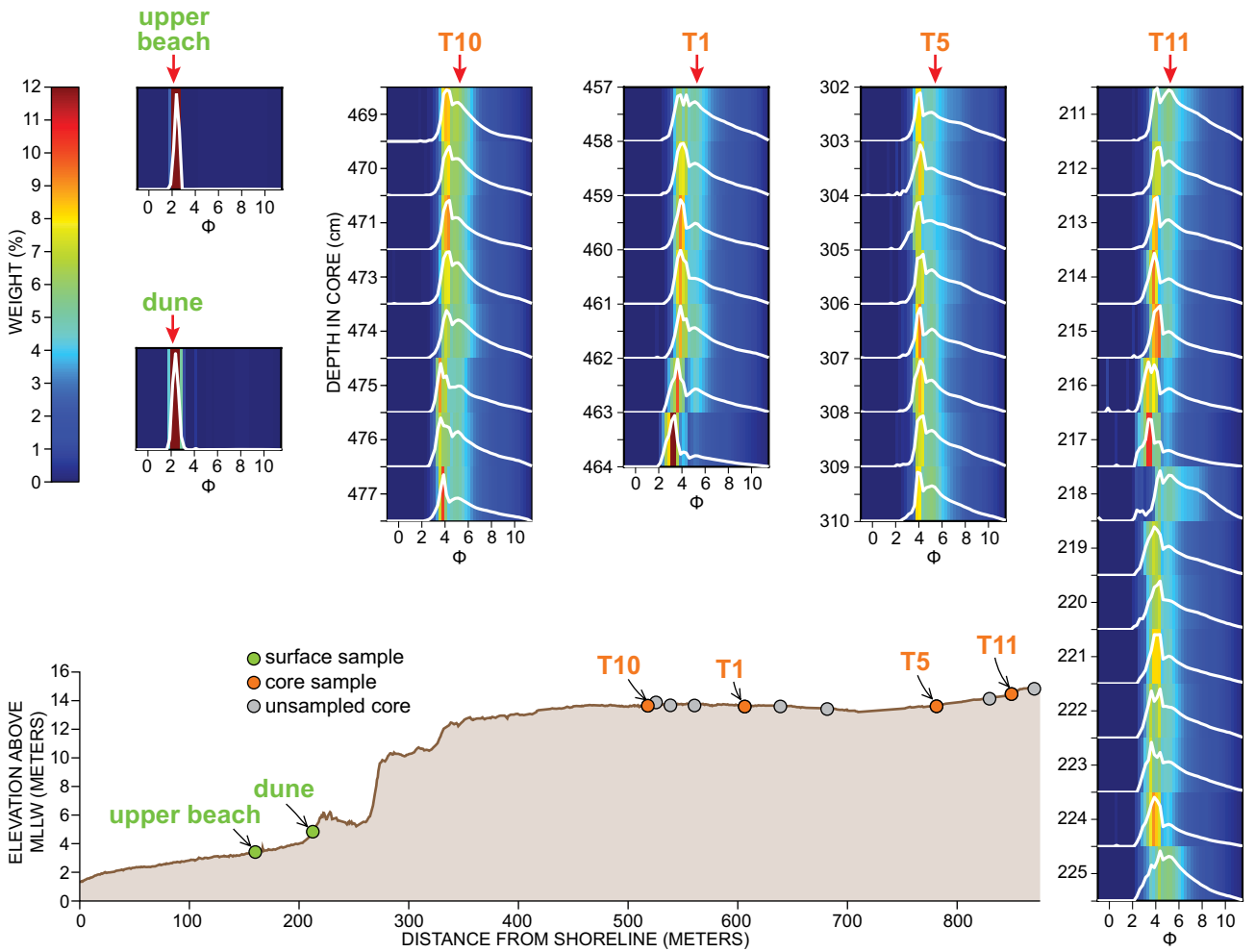

Figure 7. Changes in grain-size distribution in bed C′ among four cores (orange labels) on the Tsunami Ramp core transect. Vertical red arrows mark mean grain-size distribution of the bed in the four cores. Grain-size distributions for modern beach and dune samples, located along the elevational transect, are also shown. MLLW—mean lower low water.

Grain-size analysis of bed C′ in four cores shows that mean grain size does not fine landward (Fig. 7). However, the increase in thickness of bed C′ in landward cores T7 and T11 suggests that the primary inundation of the Tsunami Ramp basin was by silt-laden water flowing northeast into the present-day West Lake basin, and then northwest from that basin into the Tsunami Ramp basin (Figs. 2 and 3A). The lack of fine sand—like that on the modern beach and low dunes just behind it (Table S2 in the Supplemental File [see footnote 1])—in bed C′ is consistent with inundation across a landscape blanketed with silty tephra 2.

A second, 5–30-mm-thick bed (Y) of clean very fine to fine sand also has multiple characteristics typical of tsunami deposits. Bed Y maintains relatively uniform thickness as it rises landward from 10.2 to 13.4 m (Fig. 4) and grades gradually upward from very fine sand to silty sand in cores T1, T2, and T6, probably reflecting differential settling during suspension deposition (Table S2 in the Supplemental File [see footnote 1]). Bed Y sharply overlies peat in all axial cores (Table 1). Rip-up clasts in bed Y in core T7 suggest erosion of previously deposited sediment.

Two other thin beds, just above bed Y in most cores, are probably also tsunami deposits. Beds X and W are less distinct with more variable lithologies than bed Y, but contacts for both beds are sharp in two-thirds of the cores where the beds are found (Table 1). We correlate bed W along the entire core transect, whereas bed X was identified only in the seven landward cores (Fig. 4). Normal grading from sand to silt or silty sand in beds W and X probably records suspension deposition (e.g., Morton et al., 2007; Jaffe et al., 2012).

The two youngest sandy beds (v and *j*, Fig. 6) at the site may or may not have been deposited by tsunamis. Bed v is lithologically similar to bed W, but with more gradational contacts, probably due to root mixing. As shown on CT X-ray scans, the 15–20 mm of peat in cores T5, T8, and T11 that separates each of these four closely spaced beds (Y, X, W, and v) from each other shows that the beds record four separate events decades apart (at rates of peat deposition discussed in the following). Bed *j* was found in too few cores (T11, T6) to infer its genesis.

Three beds of silty peat to peaty very fine sandy silt found in three to four cores are probably not tsunami deposits. Bed S has sharp lower contacts in cores T8 and T9, but CT X-ray scans of core T11 show that beds *z* and *a*′ have more gradational contacts than most other beds (Table 1; Fig. 6). Smear slides from these three beds reveal an abundance of elongate, angular, silt-sized grains, many of which are glass. Because these beds have the same orange hues (Munsell 5YR) as tephra 2, they probably contain reworked tephra (Table 1), perhaps from now-buried outcrops of tephra 2 along the northeast edge of the Tsunami Ramp basin.

The oldest possible tsunami deposit, bed d′, was correlated among the five landward cores (Table 1; Figs. 4 and 6). Although of variable silty lithology, its light gray color, massive structure, and sharp lower contact in four cores suggest suspension deposition.

Beds of clayey to sandy silt a few centimeters thick cap silty diamicton near the base of half the axial cores. Based on ^{14}C ages from cores T10 and T11 (Fig. 4; Table 3) the silty beds are pre-Holocene; we infer that they are proglacial or immediately postglacial pond or lake deposits rather than tsunami deposits.

Drained Lake Site

Lithofacies exposed in a transect of 8 cores along the axis of a gently sloping (6–16 m elevation), 150-m-wide, peat-covered alluvial fan at the Drained Lake site (site D), on the east edge of Drained Lake basin, consist of thin sandy beds within a sequence of 3–4 m of freshwater peat (Figs. 2 and 3B). Radiocarbon ages date the peat sequence to the past 3500 yr (Fig. 5; Table 3; Table S3 in the Supplemental File [see footnote 1]). In contrast to most beds at the Tsunami Ramp site, beds at the Drained Lake site largely consist of fine to very fine sand; the most well-sorted beds contain more fine than very fine sand and minor amounts of medium sand (Table 2). Grains are mostly equidimensional quartz, feldspar, and rock fragments, with few of the elongate, silt-sized grains common in beds at the Tsunami Ramp site. The mean grain size of most Drained Lake sand beds is similar to sand from the modern beach and dunes 600–700 m to the southwest (Fig. 2), but core samples are less well sorted (Table S2 in the Supplemental File [see footnote 1]). With a few exceptions where upper and lower parts of sand beds are mixed with peat, upper and lower contacts are sharp to very sharp (usually 1–3 mm; Table 2). Contacts of the few silty (usually peaty) beds are more gradual. No tephra beds were identified at the Drained Lake site.

Based on our correlations (Fig. 5), 28 sandy to silty beds, potentially deposited by tsunamis, were identified in transect cores at the Drained Lake site. Sandy beds that could not confidently be correlated to at least one other core were not considered further, leaving 20 beds (Table 2). Most of the uncorrelated beds were in the highest core (D5), collected where the canyon that feeds the fan widens (Fig. 3B). Although the well-sorted sand in some of the core D5 beds suggests that they are potential tsunami deposits, the poor sorting and angular clasts in others point to transport from higher elevations and deposition by streams or debris flows. Based on the distribution and distinctness of characteristics typical of tsunami deposits (Table 2), we group the remaining 20 beds into probable tsunami deposits (13), possible tsunami deposits (6), and non-tsunami deposits (1; Table 2; Figs. 5 and 8).

The nine most extensive probable tsunami deposits (uppercase letter labels in Table 2; Fig. 8) have characteristics similar to those of tsunami deposits described from peat or soil sequences landward of sandy beaches (e.g., Dawson and Smith, 2000; Gelfenbaum and Jaffe, 2003; Bourgeois et al., 2006; Jankaew et al., 2008; MacInnes et al., 2009; Sawai et al., 2012; Szczuciński et al., 2012), where sheets of clean sand less than a few centimeters thick can be mapped for hundreds of meters inland. Beds D, H, I, and N rise 7–8 m along the 265 m length of the core transect; even the deepest beds of this group, found only in a few cores, extend at least 100 m (Fig. 5). In most cores, these distinct beds consist of clean, well-sorted very fine to fine sand at least 10 mm thick with very sharp to sharp contacts. We noted normal fining-upward grading in six of nine beds (Table 2). In core D5, the fine sand of bed D grades upward into sandy silt, reaching a thickness of 65 mm at an elevation of 15 m. Based on its stratigraphic position, the clean sand of bed N in cores D2, D3, and D8 correlates with gravelly silty sand in core D6 and a silty diamicton in core D7; the poor sorting and angular clasts in the correlative beds in these latter cores suggest that the beds are stream and debris-flow deposits contemporaneous with deposition of sand by a tsunami. Another 4 less extensive probable tsunami deposits (beds E, K, O, and S; Table 2; Fig. 8) are sandy with generally sharp contacts, but they correlate among only 4 of the 8 cores and do not rise above 10 m. Relative to the more extensive beds of this group, these less extensive beds tend to be siltier and more are mixed with peat.

We label six other beds (b, f, g, m, t, and u) of sand to peaty sand as possible tsunami deposits because they contain a higher proportion of peat in some cores than the beds discussed above and/or are found in too few cores (only two to four) to fully evaluate. The silty texture, poor sorting, and angular clasts in bed *l* in cores D6 and D7 suggest that the bed was deposited by a stream rather than a tsunami.

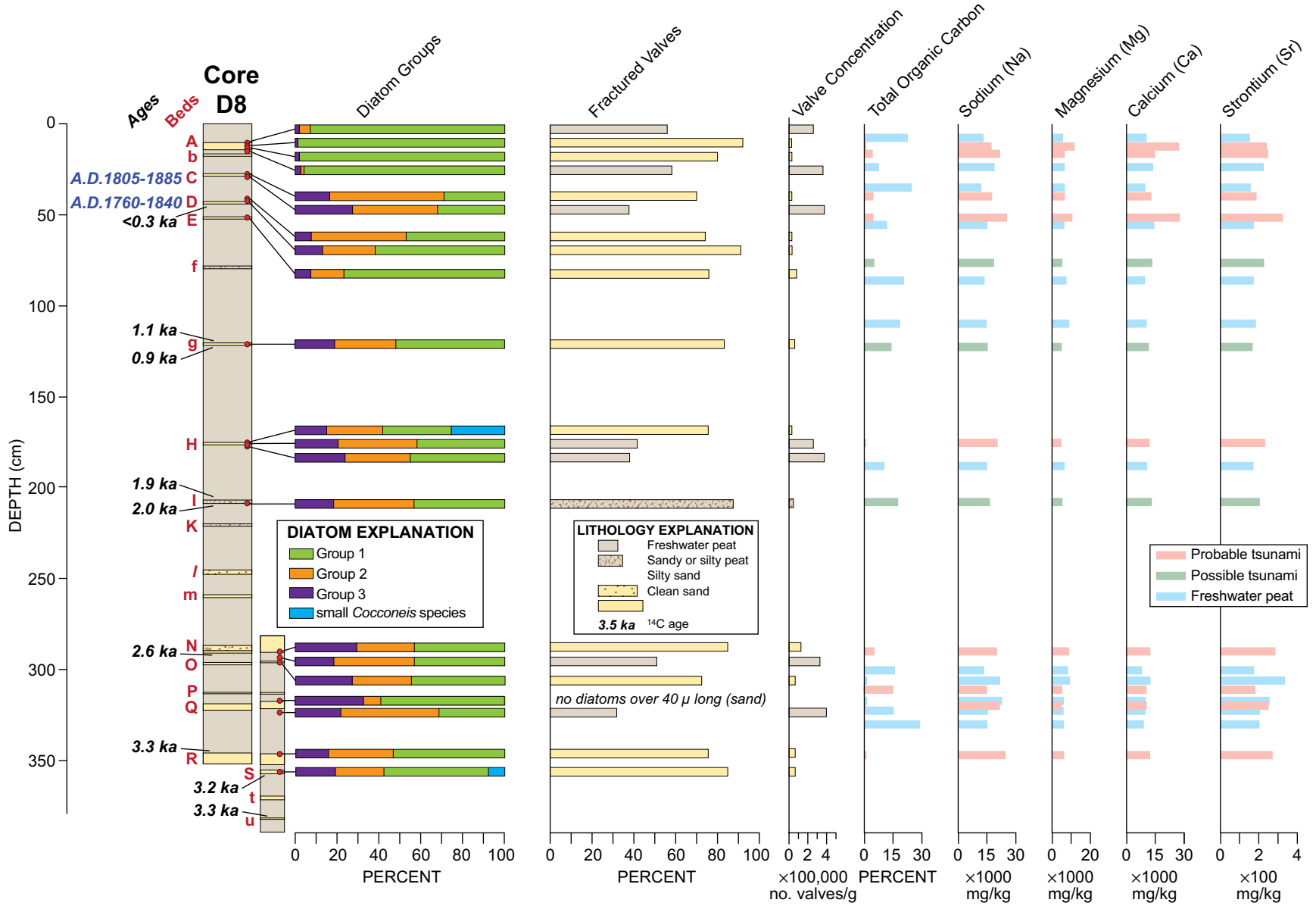

Figure 8. Core D8 at the Drained Lake site showing lithology and optically stimulated luminescence and key accelerator mass spectrometer ^{14}C ages (see Tables 3 and 4), and selected diatom and geochemical data for samples from the core (complete data in Supplemental File [see footnote 1]). Bed labels as in Table 2. Diatom samples were analyzed from sand beds and adjacent peat. Diatoms are grouped according to their preferred habitat. Group 1—benthic diatoms commonly found in acidic, freshwater peat bogs (e.g., Rühland et al., 2000). Group 2—four species of *Aulacoseira*, a freshwater planktonic genus commonly found within freshwater peat diatom flora (Crawford et al., 2003). Group 3—small, tychoplanktonic alkaliphilous taxa commonly found in shallow freshwater environments (Brugam and Swain, 2000; Tingstad et al., 2011). Colors of bars in the Fractured valves column show the lithology of diatom sediment samples. Colors of bars showing geochemical analyses on the right indicate samples from probable and possible tsunami deposits (Table 2) and peat.

Potential tsunami deposits were not identified in core D9 below the 5–6-m-high shorelines, 130 m northwest of core D3 (Fig. 3B). After many attempts to core through resistant sand, we recovered only 0.5 m of fine, well-sorted sand overlying 0.5 m of interbedded peaty silt, silty peat, and fine sand (Fig. 9). The grain-size distribution of sand in the upper half of the core is very similar to a sample from low dunes 400–500 m to the southwest (Table S2 in the Supplemental File [see footnote 1]). Stratigraphy in several cores at the site of D9 is too inconsistent to correlate the sandy beds of core D9 with those of the core transect to the east. Based on the wide distribution of modern sand deposits in Drained Lake basin, at least the upper sand beds in core D9 are probably wind and stream deposits reworked by the shallow lakes and ponds that have occupied the basin.

Diatom assemblages of samples from core D9 are dominated by freshwater species typical of shallow lakes, peat bogs, and muskeg (Fig. 9). However, two sand samples and one of mud contain significant (15%–25%) numbers of species of the genus *Cocconeis* and small numbers (<1% relative abundance) of the brackish-water species *Tryblionella debilis* and *Surirella brebissonii* (small *Cocconeis* species group in Fig. 9; Tables Sda1 and Sda2 and Fig. Sda3 in the Supplemental File [see footnote 1]). These salt-tolerant benthic species, common in tidal environments (e.g., Hemphill-Haley, 1995), have also been reported from lakes. Their presence in core D9 with the absence of other species typically found in brackish estuaries or lagoons may reflect infrequent tidal inundation of the former lake in Drained Lake basin.

Reconnaissance Sites

Field descriptions and photographs of 3 gouge cores at the Belligerent Bull site, 1.5 km inland at an elevation of 7–10 m (site B, Fig. 2), show a 3-m-thick upper sequence of sandy and silty beds in freshwater peat, much like the sequence in cores D1 to D3 at Drained Lake, and a lower 1.3-m-thick sequence of beds that closely matches that in the lower meter of core T11 at Tsunami Ramp (composite section in Fig. 10). Sandy beds correlate well in the 3 cores to a depth of 2.4 m, where core B1 stops. The section from 2.4 to 3.1 m in core B2 is missing in core B3, suggesting an erosional unconformity. The thick fining-upward sandy silt described in core T11 (Fig. 7; Fig. S3 in the Supplemental File [see footnote 1]; bed C′ in Table 1) is 8 and 14 cm thick in cores B2 and B3, respectively, where it overlies tephra 2. Below tephra 2, core B3 contains a 20-mm-thick orange silty bed that is probably tephra 1 and a 130-mm-thick fining-upward silty sand at its base. Core B3 extends stratigraphically 0.6 m below core B2, but core B3 is 2–3 m higher and its section is compressed relative to the other cores.

At New Ranch valley (Fig. 1C), 4 gouge cores spaced along the axis of the valley at ~7–10 m showed 0.5–1 m of freshwater peat, overlying 0.1–0.3 m of peaty mud and/or mud, overlying clean medium to fine sand at 0.5 m to 1.5 m depths. The basal sand may be tidal or perhaps contemporaneous with the vegetated dunes on the margins of the valley. In a middle valley core, 2 sand beds are found within the peat: a 4-cm-thick, fining-upward silty sand at 15 cm depth, and a 2-cm-thick clean sand at 35 cm. Silty sand beds at 0.2–0.3 m in 2 other cores may correlate with the younger of the 2 sand beds in the middle core. Because well-sorted sand lies beneath the valley floor, the sand beds may have been deposited in the channel of the small stream as well as by tsunamis spreading beach or dune sand across the valley floor. Despite the southwest orientation of this small valley, the height of the valley floor and the berm and dunes at its mouth (which may have been higher and more continuous in the past) apparently prevented most tsunamis from depositing extensive sand beds in the valley.

Attempts to Confirm a Marine Source for Potential Tsunami Deposits

Diatom Analysis

The presence of diatoms typical of marine or brackish-water environments is usually an unambiguous indicator of marine inundation (Dawson et al., 1996; Hemphill-Haley, 1996). When assemblages contain significant percentages of marine or brackish-water diatoms mixed with species that prefer freshwater environments, particularly at sites beyond the reach of storm waves, deposition by tsunamis is the best explanation for assemblage composition (e.g., Hemphill-Haley, 1995; Hutchinson et al., 1997; Nelson et al., 2008; Sawai et al., 2009; Goff et al., 2012; Chagué-Goff et al., 2015). Studies of modern tsunami deposits have shown, however, that marine diatoms may be so diluted by nonmarine diatoms that no marine taxa can be identified. Sources of the nonmarine diatoms include the freshwater to brackish-water environments of plains, lakes, and river channels that a tsunami traverses inland of the shore. For example, no marine and few brackish-marine diatoms were observed in sandy beds laid down on the Sendai plain by the Tohoku-Oki tsunami of 2011 (Szczuciński et al., 2012). Grain-size analyses of the Tohoku beds showed that within 1 km of the coast, tsunami deposits were derived mainly from the beach and coastal dunes, and because coastal sediments contained few diatoms, the tsunami-deposit assemblages were composed of mostly brackish-water and freshwater species sourced from the coastal plain.

Our analysis of diatoms in selected samples from potential tsunami deposits and adjacent peat at the Tsunami Ramp (cores T11 and T1) and Drained Lake (cores D8 and D9) sites found abundant freshwater and freshwater–brackish water taxa, very few brackish-water taxa, and no marine taxa (Figs. 6, 8, and 9; tables and figures in the Diatom Appendix (da) part of the Supplemental File [see footnote 1]). We used standard diatom preparation methods (Charles et al., 2002; e.g., Atwater and Hemphill-Haley, 1997; Sawai et al., 2009; additional information on methods in the Diatom Appendix in the Supplemental File [see footnote 1]) on 21 samples from potential tsunami deposits and 11 from adjacent peaty sediment. We identified 120 species in counts of >200 diatom valves per sample at high magnification (1000×) with reference to Krammer and Lange-Bertalot (1986, 1988, 1991a, 1991b).

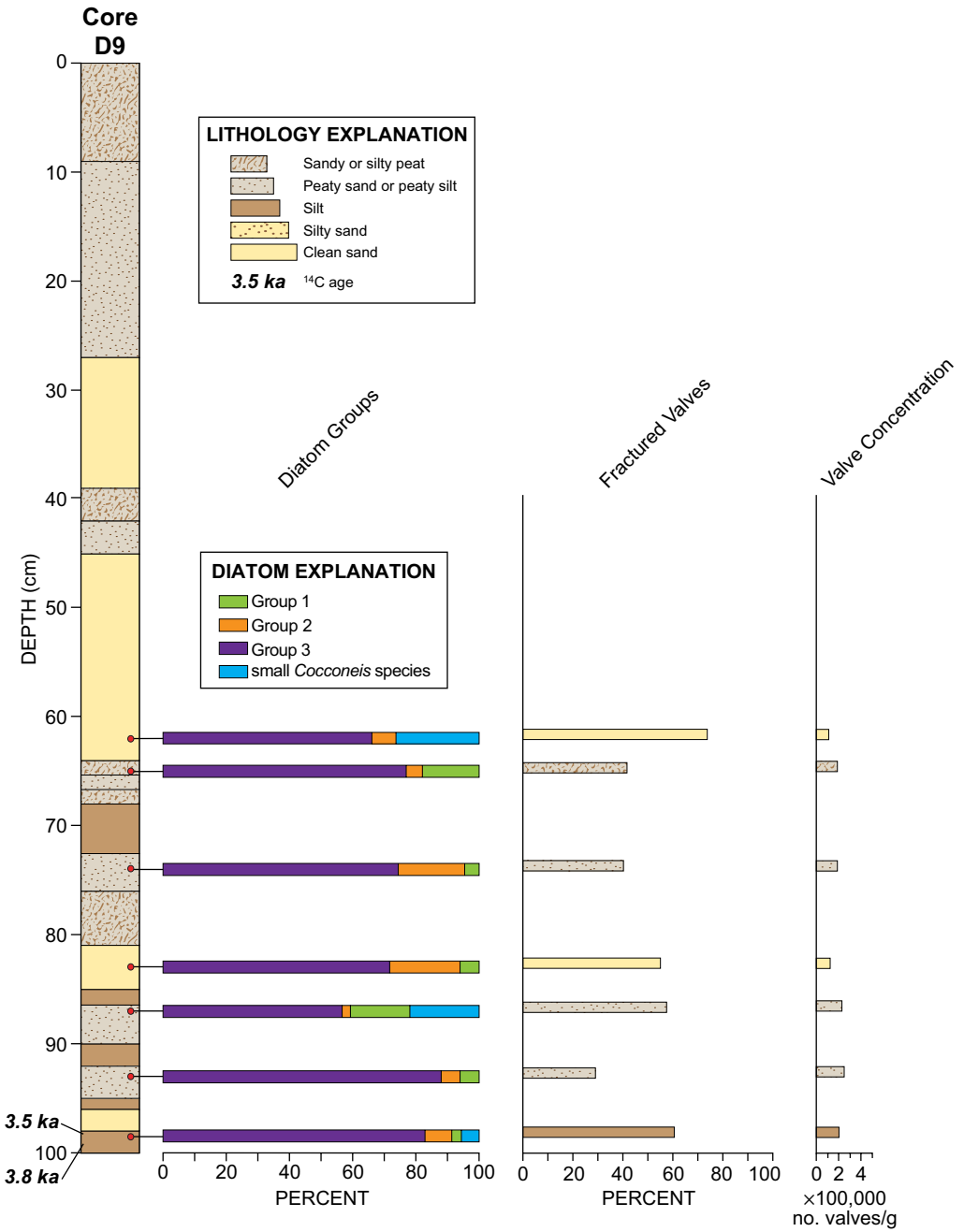

Figure 9. Core D9 at the Drained Lake site showing lithology, two ^{14}C ages (Table 3), and selected diatom data for samples from the core (complete data in Supplemental File [see footnote 1]). Diatoms are grouped according to their preferred habitat. Group 1—benthic diatoms commonly found in acidic, freshwater peat bogs (e.g., Rühland et al., 2000). Group 2—four species of *Aulacoseira*, a freshwater planktonic genus commonly found within freshwater peat diatom flora (Crawford et al., 2003). Group 3—small, tychoplanktonic alkaliphilous taxa commonly found in shallow freshwater environments (Brugam and Swain, 2000; Tingstad et al., 2011). Colors of bars in the Fractured Valves column show the lithology of diatom sediment samples.

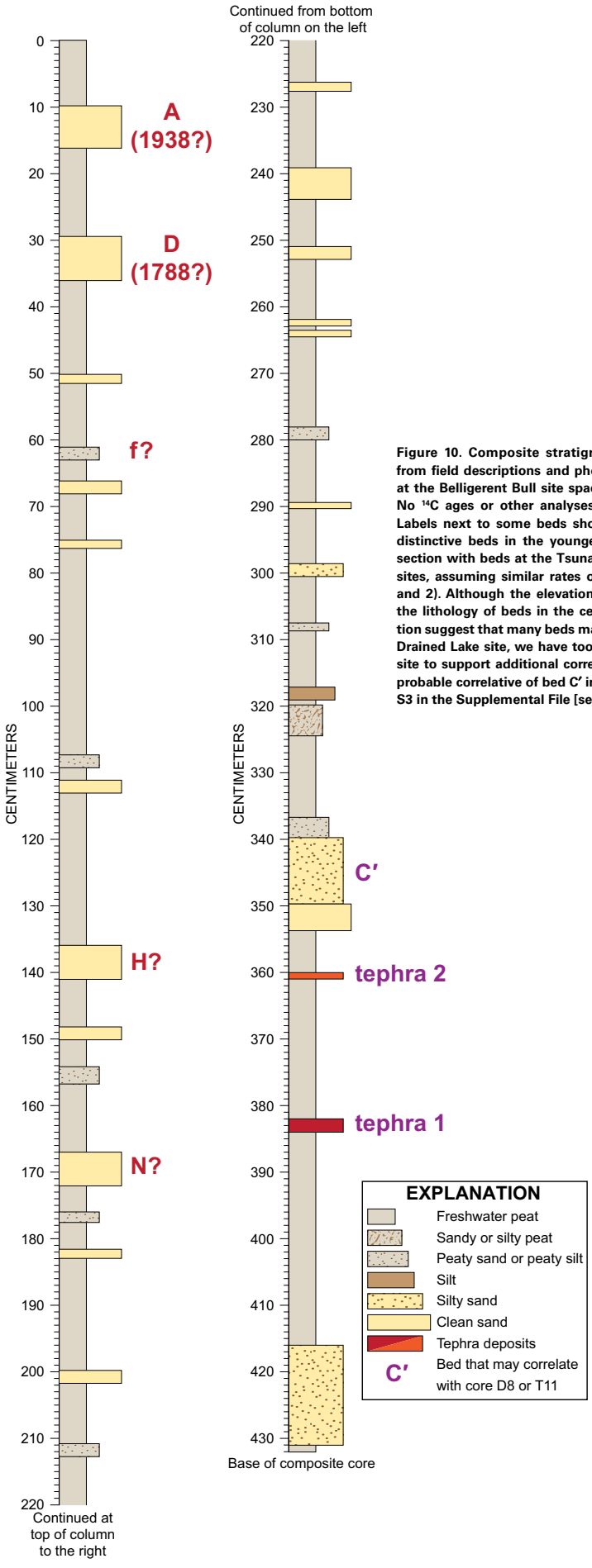

Figure 10. Composite stratigraphic section constructed from field descriptions and photographs of 3 gouge cores at the Belligerent Bull site spaced 50–120 m apart (Fig. 2). No ^{14}C ages or other analyses are available for this site. Labels next to some beds show probable correlations of distinctive beds in the youngest and oldest parts of the section with beds at the Tsunami Ramp and Drained Lake sites, assuming similar rates of peat deposition (Tables 1 and 2). Although the elevation of this site (~7–10 m) and the lithology of beds in the central two-thirds of the section suggest that many beds may correlate with beds at the Drained Lake site, we have too little information from this site to support additional correlations. (A photograph of a probable correlative of bed C′ in core B3 is shown in Figure S3 in the Supplemental File [see footnote 1].)

Ecological classifications of diatoms were based on their salinity preference and life form following Krammer and Lange-Bertalot (1986, 1988, 1991a, 1991b), Vos and de Wolf (1988, 1993), Denys (1991), Hartley et al. (1996), and Shennan et al. (2007, 2010). In addition, we scanned diatom slides at low magnification (400×) to determine whether diatoms were fractured during turbulent flow (e.g., Witter et al., 2009).

To facilitate paleoecological interpretation, we grouped diatoms based on their preferred habitat. Group 1 includes benthic diatoms commonly found in acidic, freshwater peat bogs (e.g., Rühland et al., 2000). Group 2 consists of four species of *Aulacoseira*, a freshwater planktonic genus commonly found within freshwater peat diatom flora (Crawford et al., 2003). Group 3 contains small, tychoplanktonic alkaliphilous taxa that are commonly found in shallow freshwater environments (Brugam and Swain, 2000; Tingstad et al., 2011; Figs. 6, 8, and 9).

With three possible exceptions, a comparison of the proportions of the three diatom groups (as well as individual species assemblages, Tables Sda1–Sda3 and Figs. Sda1–Sda3 in the Supplemental File [see footnote 1]) among probable tsunami deposits, possible tsunami deposits, and adjacent freshwater peat shows no consistent differences between potential tsunami-deposited beds and other sediment (Figs. 6 and 8). The peat bog (Groups 1 and 2) and shallow water (Group 3) diatoms, which are abundant in peat samples from core D8, were probably living in small pools or ponds on peaty muskeg fringing the former lake in Drained Lake basin. This environment was likely the source of the similar diatom assemblages found within the sandy potential tsunami beds as tsunamis flooded the Drained Lake basin and entrained and deposited freshwater and freshwater–brackish-water peat bog and shallow-water diatoms.

The exceptions are the *Cocconeis neodiminuta* valves found in beds H (25% relative abundance) and S (8% abundance) in core D8 and the *Tryblionella debilis* (6% relative abundance) and *Surirella brebissonii* (9% relative abundance) valves found in bed C′ in core T1 (Figs. 6 and 8; Tables Sda1 and Sda2 and Figs. Sda1 and Sda2 in the Supplemental File [see footnote 1]). *C. neodiminuta*, an epipsammic (attached to sand grains) species found in the sediment of freshwater lakes (e.g., Clague et al., 2004), is also abundant in sandy to silty samples from core D9 from the Drained Lake basin (Fig. 9; Table Sda2 and Fig. Sda3 in the Supplemental File [see footnote 1]). We infer that in the past 3.5 k.y. the former lake in the basin never rose as high as the site of core D8 (8 m); a lake this high would require a >600-m-long dam of dunes 6 m higher than the dunes bounding the basin's southwest edge today. Thus, the presence of *C. neodiminuta* in beds H and S in core D8 suggests that this species was transported to the core site from a lower, shallow lake in Drained Lake basin during tsunami inundation.

The relatively high abundance of the brackish coastal diatoms *T. debilis* (6%) and *S. brebissonii* (9%) in sand bed C′ in core T1 is unambiguous evidence for a marine incursion into the Tsunami Ramp basin (Fig. Sda1 in the Supplemental File [see footnote 1]). *T. debilis* and *S. brebissonii* were also found in core D9 in the Drained Lake basin, but the low abundance (<1%) of the brackish taxa in core D9 suggests that they were not in situ and were transported from a higher salinity environment.

The low concentration and high fragmentation of diatom valves found in potential tsunami deposits in cores T11 and D8 is typical of diatom assemblages in sandy tsunami deposits described elsewhere (Figs. 6 and 8; Sawai, 2002; Dawson, 2007; Sawai et al., 2008; Kokociński et al., 2009; Witter et al., 2009; Szczuciński et al., 2012; Chagué-Goff et al., 2015). From the absence of diatoms in three modern beach and dune samples at Southwest Anchorage (Fig. 2; Table S2 in the Supplemental File [see footnote 1]), we infer that deposits in core D8 were derived mainly from dune and beach sediment and that freshwater and freshwater–brackish-water diatoms were entrained as tsunamis flooded Drained Lake basin. We interpret the large proportions of fragmented diatoms in the sand beds at the Drained Lake and Tsunami Ramp sites as evidence for transport by turbulent flows during tsunami inundation and drawdown (e.g., Dawson, 2007; Kokociński et al., 2009; Witter et al., 2009; Szczuciński et al., 2012; Chagué-Goff et al., 2015). The most fragile >100 µm valves (*Ulnaria* sp., *Pinnularia* sp., *Cymbella* sp.) showed the highest degree of fragmentation (mean 92%; range 77%–100%), consistent with transportation during turbulent flow (e.g., Dawson, 2007). Although chemical and mechanical processes (e.g., dissolution, compaction) can fracture diatoms in situ, as shown by the relatively high percentage of broken valves in peat samples from core D8 (mean 44%; range 32%–58%), the percentage of fragmented valves was consistently higher in the sand beds (mean 77%; range 71%–93%; e.g., Cooper et al., 2010).

Samples from potential tsunami deposits at the Tsunami Ramp site contained lower diatom concentrations than samples at Drained Lake (Figs. 6, 8, and 9; Table Sda3 in the Supplemental File [see footnote 1]). Samples from bed Y in core T11 contained no diatoms. Samples from the lower half of bed C′ contained few to no diatoms, whereas concentrations of freshwater diatoms in samples from the upper one-third of the deposit were similar to those in core D8. The upward fining and higher concentrations of valves may reflect decreasing flow velocity due to ponding in the Tsunami Ramp basin following tsunami return flow (e.g., Sawai et al., 2009; Szczuciński et al., 2012).

The four youngest samples from core D8 show much smaller proportions of the shallow freshwater group and *Aulacoseira* sp. groups than older samples, suggesting a major change in site conditions in the past century and a half (dating this section of the core is discussed in the following). The decrease in species abundance in these groups reflects an increase in species of *Cymbella*, particularly the epiphyte *C. descripta* (Table Sda2 and Fig. Sda2 in the Supplemental File [see footnote 1]). In shallow alkaline lakes of the high arctic such changes have been attributed to regional climate warming (e.g., Paul et al., 2010). At the site of core D8, however, this change more likely reflects drier site conditions due to the lowering of the groundwater table during the draining of the former lake.

Geochemical Analyses

Chemical indicators of a marine source for possible tsunami deposits have been sought for decades (e.g., Minoura and Nakaya, 1991; Chagué-Goff and Goff, 1999; Chagué-Goff, 2010; Chagué-Goff et al., 2011, 2015; Pilarczyk et al.,

2012; Ramírez-Herrera et al., 2012). High concentrations of salts that are abundant in seawater, such as Na, Mg, Ca, K, Sr, or Ba, have commonly been inferred to indicate a marine source. However, depending on many site factors and the lithology of tsunami beds and host sediment, other elements such as the nonmetals S, Cl, B, Se, Br, and I, the metalloids B, As, and Sb, and the heavy metals Cd, Cu, Cr, Fe, Ni, Pb, and Zn have also been used as evidence for a marine source (Chagué-Goff, 2010; Chagué-Goff et al., 2012). Leaching due to high rainfall may remove more soluble compounds within a few years, but some elements may move into soil horizons or peat directly underlying tsunami deposits and form less soluble organic compounds (Szczuciński et al., 2007; Chagué-Goff et al., 2011). All authors agree that the concentrations of elements in tsunami deposits are highly interdependent on source water chemistry, site geology and geomorphology, climate, sediment lithology, tsunami flow characteristics, and burial history.

As explained in Table S6 and Figure S5 in the Supplemental File [see footnote 1]), we analyzed 37 samples of potential tsunami deposits and their host sediment from cores D8 and T11 to determine if differences in 56 element concentrations might suggest a marine source for potential deposits (e.g., Figs. 6 and 8). However, analysis (R statistics packages; Coghlan, 2013; Knell, 2013) of the geochemical data failed to identify differences in concentrations of elements that clearly confirm a marine source for potential tsunami deposits. Tsunamis advancing inland across the wet or snow-covered landscapes at Southwest Anchorage would quickly be diluted by abundant freshwater from lakes, streams, and boggy muskeg. In addition, the island's nearly continuous precipitation would probably flush seawater-derived soluble elements, such as Na, Mg, and Ca, from peat and sandy beds. Perhaps some of the higher concentrations of S, K, Cu, As, Se, and Cd in peat samples partly reflect a marine source for overlying beds. However, the small number of potential tsunami deposit samples from the two cores, the lack of more than one sample from any individual bed, and the tephra-rich lithology of samples from core T11 make such inferences speculative.

Dating

We estimated the age of prehistoric (all but the four youngest beds, which probably postdate the mid-eighteenth century, as discussed in the following) potential tsunami deposits at Southwest Anchorage with accelerator mass spectrometer ^{14}C ages on plant macrofossils in peat (methods described in notes to Table 3; Table S3 in the Supplemental File [see footnote 1]; Fig. 11). We narrowed the precision of our estimates by assuming that rates of peat deposition were uniform within the intervals between dated beds. Uniform rates are supported by thorough descriptions of dated cores in the laboratory, which showed no major downcore changes in peat lithology. For potential tsunami beds with maximum and minimum ages, we followed many studies (e.g., DuRoss et al., 2011; Berryman et al., 2012; Barnes et al., 2013; Shennan et al., 2014a) in using the Bayesian software program OxCal (Bronk Ramsey, 2009; Lienkaemper and Bronk Ramsey, 2009) to calculate a probability distribution for the times between our youngest maximum ages and oldest minimum ages (ages in bold in Table 3). We constrained the times of deposition for beds with no immediately overlying or underlying ^{14}C ages, or with only maximum ages, with the V-sequence stratigraphic analysis feature of OxCal (Bronk Ramsey, 2008). Using bed ages determined with maximum and minimum ages, and other maximum ages inferred to closely predate bed deposition, we calculated peat deposition rates (with assumed errors of ±25%) for each interval between the ages. Amounts of differential autocompaction of peat within each 1–50-cm-thick interval are insignificant. Rates varied from ~1.3 mm/yr in the upper parts of cores to 0.6 mm/yr in the middle and lower parts. We then used all ages and peat deposition rates in stratigraphic order to calculate probability distributions for the times of deposition of each bed in cores T11 and D8 (Table 3; Fig. 11; e.g., Kelsey et al., 2005; Goldfinger et al., 2012). At the Drained Lake site, calibrated age intervals for four beds are narrowed by interpolating rates of peat deposition between dated beds, and rates are also used to estimate time intervals for eight undated beds (Fig. 11).

The ages of two of the four youngest beds in core D8, which are too young to usefully date with standard ^{14}C methods (e.g., Kemp et al., 2013), were determined using optically stimulated luminescence (OSL) methods. We used single aliquot regeneration protocols (Murray and Wintle, 2003; Wintle and Murray, 2006) to estimate the apparent equivalent dose of the 250–150 μm quartz fractions in many tens of separate aliquots (Table 4; e.g., Wright et al., 2011; Brill et al., 2012; Prendergast et al., 2012). Very fine grains of sand from the upper 2 mm of sampled beds were selected for analysis because the uppermost grains are most likely to have been exposed to light following deposition. We assume that quartz grains in core D8 were not uniformly solar reset because of the short distance of transport. We measured ~20–40 quartz grains on each aliquot to isolate the youngest, fully solar-reset grain population. Probably <20% of grains (4–8) on each aliquot emitted enough light for measurement. Additional discussion of the OSL analyses is in the Supplemental File (see footnote 1).

Two OSL samples gave post–seventeenth century ages that agree closely with ages inferred from rates of peat deposition interpolated between ^{14}C ages (Fig. 11), although the OSL ages have >10% analytical uncertainties. The ages are also consistent with time intervals that we infer for the four youngest potential tsunami deposits through analysis of historical information about Chirikof Island (discussed in the following). A third OSL sample, from the 1.1 ka bed g in core D8, yielded insufficient light levels to calculate an age.

Alternative Processes

We considered four non-tsunami processes for probable and possible tsunami deposits at the Tsunami Ramp and Drained Lake sites: deposition by (1) wind-generated waves, (2) wind, especially melt out of sandy beds that accumulated on snow in winter, (3) streams as channel deposits, and (4) debris

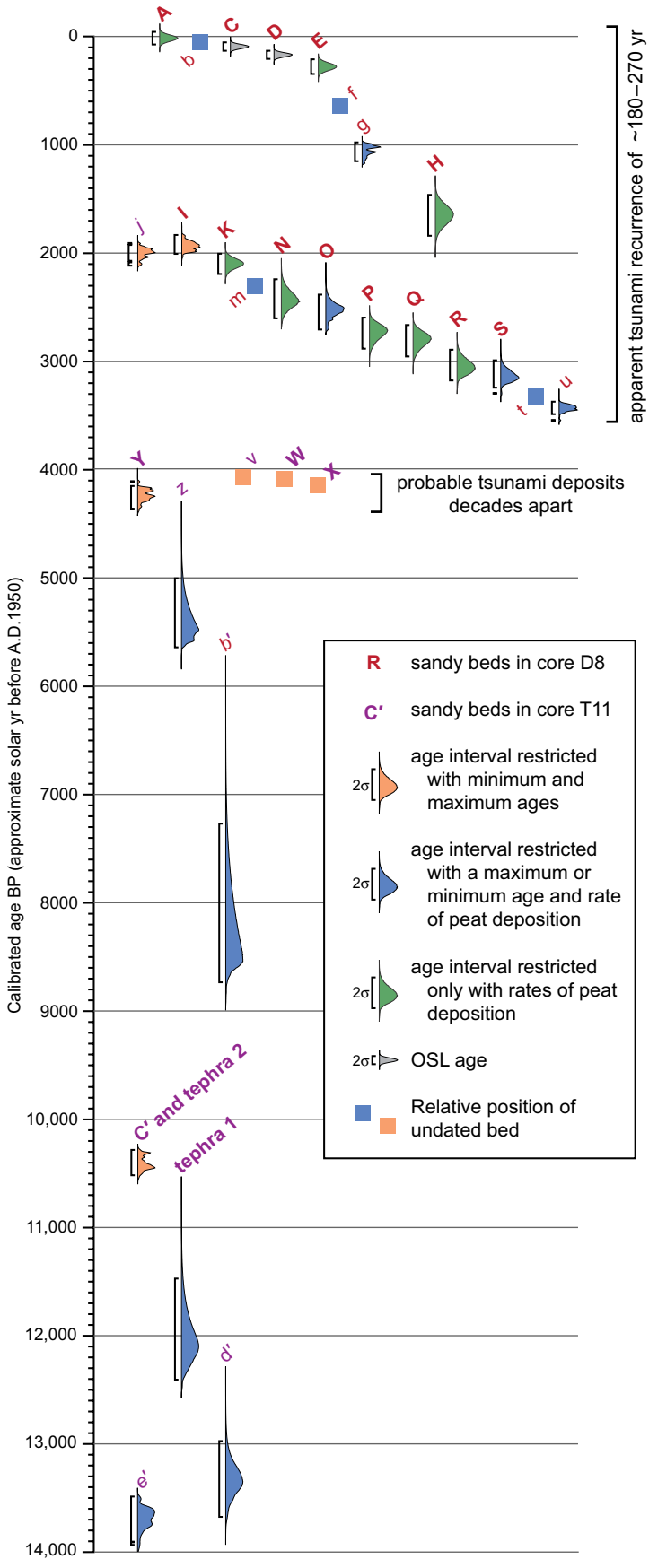

Figure 11. Age probability distributions for probable (bold uppercase letters) and possible (lowercase letters) tsunami deposits from cores D8 (red) and T11 (purple) calculated using the V-sequence feature of OxCal (Bronk Ramsey, 2008; program code in Table S4 in the Supplemental File [see footnote 1]). Distributions limited by maximum and minimum ^{14}C ages (Table 3) are in orange, those with only a maximum or a minimum age are in blue, and distributions calculated using only interpolated rates of peat deposition are in green. Two optically stimulated luminescence (OSL) age distributions are in gray. The relative position in the stratigraphic sequence of possible tsunami deposits without maximum or minimum ages from core D8 are marked by blue squares. Orange squares indicate three beds in core T11, separated by only a few centimeters of peat, suggesting that they were deposited within decades of each other. Average recurrence of tsunamis inferred for the past 3500 from core D8 varies from ~180 yr (possible and probable deposits) to ~270 yr (only probable deposits; mean recurrence ± 1σ calculated with OxCal is 262 ± 238 yr.

TABLE 4. OPTICALLY STIMULATED LUMINESCENCE (OSL) AGES ON QUARTZ GRAINS FROM THREE SAND BEDS IN CORE D8

Bed label	Laboratory number	Aliquots	Equivalent dose* (Gy)	U (ppm)	TH (ppm)	K_2O (%)	H_2O (%)	Cosmic dose† (mGy/yr)[4]	Dose rate (mGy/yr)	OSL age§ (yr)
C	UIC3100	30/60	0.192 ± 0.014	1.2 ± 0.1	2.9 ± 0.1	1.04 ± 0.01	40 ± 5	0.20 ± 0.02	1.14 ± 0.06	165 ± 20
D	UIC3101	16/60	0.227 ± 0.015	1.1 ± 0.1	3.4 ± 0.1	0.89 ± 0.01	40 ± 5	0.20 ± 0.02	1.06 ± 0.06	210 ± 20
I	UIC3123	21/60	incalculable	1.4 ± 0.1	5.3 ± 0.1	0.95 ± 0.01	40 ± 5	0.16 ± 0.02	1.22 ± 0.06	incalculable

Note: Bed labels are from core D8 (as shown in Table 2). Beds consist of fine sand, 5–12 mm thick. U, Th and ^{20}K contents analyzed by inductively coupled plasma–mass spectrometry (Activation Laboratory LTD, Ontario, Canada).

*150–250 µm quartz fraction with 100–300 grains/aliquot and analyzed under blue light excitation (470 ± 20 nm) by single aliquot regeneration protocols (Murray and Wintle, 2003). Equivalent dose calculated using a residual corrected cluster analysis on the indicated aliquots (e.g., Pierson et al., 2010).

†From Prescott and Hutton (1994).

§All errors are at 1σ. Ages are from the reference year A.D. 2010, with errors that incorporate systematic and random components at 1σ.

flows. Several of these depositional processes can be dismissed at each site on the basis of lithology and site geomorphology. A tephra origin, either by air fall or reworking of tephra by slopewash, was discussed for three beds at the Tsunami Ramp site (Table 1).

Deposition by wind-generated waves can be ruled out as a depositional process for sandy and silty beds at the Tsunami Ramp site unless the island was at least 4–5 m lower relative to sea level in the past than it is now. If the island had been lower with the sea extending many hundreds of meters into Drained Lake basin in the past 3500 yr, we would expect marine or brackish-water taxa to be abundant in core D9, but no marine diatoms and few (<1% relative abundance) brackish diatoms were found in the 3 of 7 samples in core D9 whose assemblages do not consist exclusively of freshwater taxa (Fig. 9). As long as the Southwest Anchorage shoreline was within a few meters of its present elevation, even an exceptionally high storm surge could not have risen high enough (>14 m) for wind-generated waves to deposit sand beds at the Tsunami Ramp site (Figs. 3 and 4).

Wind-generated waves are a possible process for sand beds at the lower end of the Drained Lake site (7–9 m elevation), either during a high storm surge that extended many hundreds of meters into Drained Lake basin or during periods when the basin was occupied by a lake reaching the 5–6 m shorelines (Fig. 2). The lack of marine diatoms in samples from the site makes waves during a storm surge less likely than lake waves. However, the height of wind-generated waves would be quite limited because steep hills protect the Drained Lake site from the prevailing southeasterly winds. Even if winds were from the west during severe storms, the fetch across Drained Lake basin to the core transect would have been <650 m. Sand beds deposited by storm waves on a slope like that along the Drained Lake core transect typically have horizontal laminations or thin landward over distances of tens of meters (e.g., Goff et al., 2004; Morton et al., 2007), whereas most of the sand beds in transect cores lack laminations and climb the fan slope for 50–100 m with relatively uniform thicknesses (Figs. 3B and 5; Table 2). If more than a few of the sand beds had been deposited by wind waves, we would expect to find a greater number of beds in the westernmost cores than in the higher eastern cores. Because we can correlate all our probable and possible tsunami-deposited beds in the eastern cores 50–100 m inland (Table 2), we conclude that few of these beds were deposited by wind-generated waves.

Even though we lack ages for any of the sandy beds at the Belligerent Bull site (Fig. 2), the similarities in the stratigraphic sequence in the upper 3 m at this site with the Drained Lake core stratigraphy (Figs. 2B, 8, and 10) suggests that at least some of the Drained Lake beds extend an additional kilometer inland to this site. Because the Belligerent Bull cores are 200–350 m east of the 5–6 m shorelines (Fig. 2), a wind-generated wave origin for their sandy beds is very unlikely.

Eolian transport is a second possible process for the deposition of sand beds at the Tsunami Ramp and Drained Lake sites. Unconsolidated sand covers much of the western third of the island; low dunes and blowouts are widespread features along the southwest coast and in Drained Lake basin; and strong winds blow year round, probably exceeding velocities of 150 km/h in winter. At our muskeg sites, sand deposited by the wind in summer would be rapidly mixed with and infiltrated into peat without forming distinct beds. Laboratory descriptions and smear slides in cores at both sites show trace amounts (<<1%) of very fine to fine sand in much of the peat in the cores. In winter, however, sand might accumulate throughout the snow pack and then be deposited as distinct beds onto peat as the snow melted in the spring. If snow accumulated in drifts with irregular topography, we would expect such snowmelt eolian beds to extend for less than many tens of meters, have highly variable thicknesses, lack upward grading, and display deformation features formed during melting (e.g., Ballantyne and Whittington, 1987; Koster and Dijkmans, 1988). Diatom valves would not be deposited in eolian beds, but may have infiltrated well-sorted beds from overlying peat. As none of the probable tsunami-deposited sand beds at either site have such characteristics, we dismiss wind accumulation with snowmelt as the origin of probable beds. We cannot, however, rule out wind accumulation with snowmelt for some of the possible tsunami-deposited sandy peat and peaty sand beds at the Drained Lake site. However, because these beds correlate with clean sand beds in adjacent cores and extend for distances of 20–100 m, they are probably not eolian.

Stream or debris-flow deposition is a viable process for the deposition of correlated beds only at the Drained Lake site. No streams drain into the Tsunami Ramp basin, basin slopes are gentle, and the drainage basin is small (<0.4 km^2; Fig. 3A). Although the steep sides (30°–40°) of the V-shaped stream valley at the apex of the Drained Lake fan are well stabilized by vegetation, occasional slumping apparently contributes enough sediment to the <1-m-wide meandering stream to form small channel deposits or debris flows (with angular clasts of local bedrock). The small size of the drainage basin (<0.4 km^2) and the thin, <0.5-m-wide channel deposits in the present stream suggest that it rarely deposits debris-flow or channel sediment more than a few tens of meters beyond the mouth of the valley. Most of the 23 sandy or silty beds in core D5 near the apex of the fan cannot be reliably correlated to beds in lower cores along the transect. For this reason, we group only the 4 clean sand beds in core D5 that we can correlate 265 m to lower cores on the transect with probable or possible tsunami deposits (Fig. 5; Table 2).

TSUNAMI HISTORY

Historical Tsunamis

In this section we use historical information from the Chirikof Island region (Semidi segment, Fig. 1B) with our OSL ages and peat deposition rates for the four youngest potential tsunami beds to suggest correlations of the beds with historically recorded earthquakes and tsunamis.

The first high tsunami in the Chirikof Island region for which we have accurate written records accompanied the first of 2 large earthquakes in 1788 that together ruptured at least 600 km of the eastern Aleutian arc (Davies et al., 1981; Soloviev, 1990; Briggs et al., 2014a, fig. 1 therein; Shennan et al., 2014b; Witter et al., 2014, fig. 1b therein). Although it is unclear if reports of severe flooding in the western part of the ruptured zone occurred following the 21 July earthquake or the later 6 August earthquake, 1 or 2 high tsunamis (reported run-up heights range from 3 to >30 m) caused much damage and many deaths from Kodiak Island to Sanak Island (Fig. 1; Lander, 1996; Ryan et al., 2012b; Witter et al., 2014). The highest tsunami inundation at Southwest Anchorage was probably on 21 July, when the tsunami severely flooded Three Saints Harbor on Kodiak Island, 215 km to the northeast. Although Alutiiq hunters may have experienced the 1788 tsunami on Chirikof Island during their seasonal harvest of ground squirrel pelts, no written accounts of the tsunami exist (a Russian hunting outpost was not established on the island until 1798; Black et al. in the Supplemental File [see footnote 1]).

Bed D at the Drained Lake site was probably deposited by the 1788 tsunami. Two ^{14}C ages suggest that the bed was deposited in the past 300 yr and an OSL age places it in the late eighteenth or earliest nineteenth century (Tables 3 and 4; Fig. 11). Bed correlations at the Drained Lake site show that bed D rises higher than the beds of other probable tsunami deposits, reaching almost 15 m (Table 2; Fig. 5). Inundation of Southwest Anchorage to >15 m is consistent with reported run-ups in 1788 and with the 1.3 km inland extent of a probable 1788 tsunami deposit dated with ^{137}Cs and ^{210}Pb methods on Sitkinak Island, 125 km to the northeast (Lander, 1996; Briggs et al., 2014a).

To correlate the three youngest potential tsunami deposits at the Drained Lake site with historically recorded earthquakes and tsunamis of the nineteenth and twentieth centuries, we used summaries of the island's history (Keithahn, 1962; Wright, 1964; Chaffin, 1967; Long, 1975; Chaffin et al., 1983; Fields, 2000; Black et al. in the Supplemental File [see footnote 1]; Clark et al. in the Supplemental File [see footnote 1]; Clark, 2010) with inferences about the length of time it took the peat separating the beds to form. In some years of the early nineteenth century, Russian-directed hunting of ground squirrels on Chirikof Island may have been seasonal, but in most years after 1798 a few to a few tens of people lived at Southwest Anchorage, and at least from 1825 to 1868 the population of Ukamuk village was 70–120 (Black et al. in the Supplemental File [see footnote 1]). As records of the number of parkas made from harvested pelts were kept throughout this period, tsunami inundation high enough to severely damage village storehouses and a chapel (built 1841–1844; we estimate that the village occupied a site <6 m in elevation) would have been recorded. Black et al. in the Supplemental File (see footnote 1) mentioned records of strong earthquakes felt at Southwest Anchorage on 18 August 1826, in June 1833, on 4 April 1847, and an extraordinary earthquake on 17–18 June 1848 (Davies et al., 1981). Although the 1847 earthquake may have ruptured a 500-km-long section of the megathrust west of Chirikof Island (Davies et al., 1981), Black et al. (in the Supplemental File [see footnote 1]) stated that they found, "No information on any damage by tidal waves or sea turbulence associated with earthquakes…."

If bed D at a depth of 43 cm in core D8 dates from 1788, as we infer, the 15 cm thickness of peat between it and the next youngest probable tsunami deposit (bed C) represents ~60–100 yr. Thus, bed C, which was deposited as high as 9.6 m in core D7, must postdate the abandonment of Ukamuk village in 1869–1870 (due to the end of Russian sovereignty in Alaska), and predate the arrival of fox and cattle ranchers after 1890.

Displacement on the fault that ruptured the southeast part of Chirikof Island during the strong earthquake of 29 September 1880 (Moore in the Supplemental File [see footnote 1]; Lander, 1996), the effects of which were described earlier, is the most likely source for the tsunami that deposited bed C. Following the 1880 earthquake several tsunamis moved inland at least 60 m, but did not apparently inundate a cabin at Southwest Anchorage 500 m inland at an elevation that we estimate as ~11–12 m (Lander, 1996, p. 46). If our mapping of this bed at the Drained Lake site is correct, the tsunami may have almost reached the cabin. Because this tsunami was not reported elsewhere and the earthquake was felt no farther than 100 km from Chirikof Island, it must have occurred on a local fault in the upper plate above the Alaska-Aleutian megathrust (Davies et al., 1981; Lander, 1996). An undocumented tsunami very early in the twentieth century is an unlikely but possible alternative for the tsunami that deposited bed C; for example, the tsunami that Black et al. (in the Supplemental File [see footnote 1]) suggested may coincide with the M ~7.7 earthquake of 10 October 1900 near central Kodiak Island.

Sources for the two youngest (twentieth century) potential tsunami deposits in the Drained Lake cores are similarly uncertain. Possible tsunami bed b is thin and indistinct, rising only to 8.3 m, whereas probable bed A is distinct, twice as thick, and climbs twice as far inland to 9.8 m (Fig. 5) in core D7. Less than 2 cm of peat separates the 2 beds in the 4 cores where they are identified, suggesting that one followed the other by only a decade or two (Fig. 11). Assuming that bed C dates from 1880, we use the 10 cm thickness of peat between beds C and b to infer that beds b and A date from the first half of the twentieth century.

For most of the twentieth century the population of Chirikof Island was probably fewer than a dozen, commonly dispersed in several locations, and in most years only seasonal; thus, inundation by tsunamis is unlikely to have been reported. From the 1890s to ca. 1915 only a few families and later only managers and their assistants, all involved in trapping introduced blue fox, lived on the island. Fox trapping continued into the late 1940s, but few dates and lengths of visits are recorded (Chaffin et al., 1983; Fields, 2000; Black et al. in the Supplemental File [see footnote 1]). John W. (Jack) McCord, who intermittently tried to establish cattle ranching on the island, first landed on the island in 1925, but his 8–9 visits in the 1930s and 1940s lasted only days to a few months (Long, 1975). By the late 1940s, the focus of cattle ranching had shifted from ships landing mainly at Southwest Anchorage to aircraft and ships landing on beaches on the central east coast of the island, where a ranch had been built 10–12 m above the beach (Fig. S2 in the Supplemental File [see footnote 1]; Keithahn, 1962; Wright, 1964; Long, 1975; Chaffin et al., 1983; Fields, 2000; Black et al. in the Supplemental File [see footnote 1]).

The largest earthquake in the Chirikof Island region since 1788 was the M 8.2 earthquake of 10 November 1938 (Davies et al., 1981; Estabrook et al., 1994; Johnson and Satake, 1994). It is unlikely that anyone was living on Chirikof Island at the time; the only reports of the height of the 1938 tsunami are <0.3 m from distances of >650 km from the island (Lander and Lockridge, 1989; Lander, 1996; Ryan et al., 2012b). The tsunami was measurable, however, as far away as Japan, and Johnson and Satake (1994) used the tsunami wave forms to estimate the earthquake magnitude as 8.2, its rupture length as 300 km, and its depth as >20 km. The modeling of Johnson and Satake (1994) showed the greatest slip on the megathrust (3.3 m) during the earthquake in the eastern quarter of the rupture zone beneath Chirikof Island. As Lander (1996, p. 64) noted, "The very small size of this tsunami for a great earthquake is unexplained."

We suggest that the 1938 tsunami in the eastern part of the rupture zone was much higher, inundating Southwest Anchorage to 10 m and depositing bed A. Shallow slip on the megathrust, even over a limited area, could produce a higher than expected tsunami, although the modeling of slip at >20 km depth by Johnson and Satake (1994) is incompatible with shallow slip. Perhaps a nearby submarine landslide increased the 1938 tsunami height, as happened following the M 8.6 April 1946 earthquake 560 km southwest of Chirikof Island (Okal et al., 2003; Fryer et al., 2004; López and Okal, 2006; Miller et al., 2014). Until more is known about the 1938 rupture, our hypothesis that its tsunami may have locally reached a height of 10 m is difficult to assess.

If possible bed b was deposited by a tsunami a decade or two prior to 1938, the best candidates are a tsunami following a M 7.9 earthquake in the Shumagin Islands, 240 km to the west in 1917, or a tsunami following a local earthquake of M 7.1 near Chirikof Island in 1923. We are not aware of reports of a tsunami following either earthquake.

The tsunami accompanying the M 9.2 earthquake of March 1964 could not have deposited bed A. Applying rates of peat deposition discussed above, the 8–15 cm thickness of peat overlying bed A suggests that it predates 1964 by at least several decades. Much of the momentum of the 1964 tsunami was directed to the south and southeast, perpendicular to the rupture zone whose southwest end was near Kodiak Island, and the tsunami did not overtop storm shorelines on Sitkinak Island, 110 km closer to the earthquake source area (Fig. 1; Plafker and Kachadoorian, 1966, p. D22).

The height of tsunami inundation on Chirikof Island in 1964 is uncertain. Black et al. (in the Supplemental File [see footnote 1]) stated "…the island was inundated by the tsunami…" and "The ranchers left.", implying that damage to cattle operations on the east coast of the island caused by the tsunami led to the departure of the ranchers. Fields (2000, p. 206) related that the ranchers reported that the tsunami on the east side of the island revealed previously never-exposed reefs. Little-decayed pieces of driftwood scattered around Drained Lake basin as high as 3–4 m may date from either 1938 or 1964.

Tsunami erosion at Southwest Anchorage in 1938, and possibly to a much lesser extent in 1964, could explain why archaeologists surveying the island in 1963 and 2005 were puzzled by the scarcity of evidence for the Russian and American occupations of Ukamuk village. Saltonstall and Steffian (in the Supplemental File [see footnote 1]) described the extensive erosion of archaeological sites near the former Ukamuk village, which occurred in the middle and later twentieth century, particularly after 1963. Of the fences, corrals, and cabin behind the beach visible in photographs from the early 1960s, only the cabin foundation remained in 2005 (Saltonstall and Steffian in the Supplemental File [see footnote 1], p. 43). An archaeologically rich meadow behind the south end of the beach, described in 1963 as 500 m by 75 m (Workman, 1969), measured only 20 by 25 m in 2005 (surface 8 m above MLLW in 2010; Fig. 3B). Saltonstall and Steffian (in the Supplemental File [see footnote 1]) attributed much of this erosion to the migration of dunes and blowouts accentuated by artifact hunters and trampling by cattle; they also inferred that sudden subsidence during the 1938 earthquake had caused waves to breach the dunes that dammed a lake in Drained Lake basin, draining the lake and exacerbating erosion of dunes and meadows between the former lake and the beach. The most recent report of a lake in Drained Lake basin, however, dates from 1893 and the size of the lake is uncertain. Subsidence during the twentieth century was more likely gradual—as GPS data show that it has been since 1995—and coseismic motions in 1938 were most likely uplift, if slip occurred on the currently locked patch of the megathrust beneath the island. If our inference that the 1938 tsunami inundated Southwest Anchorage to an elevation above 10 m is correct, tsunami return flows could have eroded the present sandy area behind the beach, transported surface evidence of occupation, and removed vegetation to expose dune and beach sand to the wind.

Prehistoric Tsunamis

Comparison of the stratigraphic sequences of potential tsunami beds at our two primary sites reveals a striking contrast in tsunami history (Fig. 11). Along the core transect at the Drained Lake site, we identified 13 probable and 6 possible tsunami deposits dating from the past 3500 yr (Table 2). However, at the Tsunami Ramp site only one possible tsunami deposit was deposited during the same period, and the lithology and limited extent of this bed are not convincing evidence of a tsunami (Table 1). The youngest bed (Y) with strong evidence for tsunami deposition at the Tsunami Ramp site predates by at least a few centuries the oldest bed at the Drained Lake site (R). The lowest cores at Drained Lake have been 6–7 m lower than cores at Tsunami Ramp over the past 3500 yr.

The topography of West Lake basin suggests that tsunamis entering the basin would access the Tsunami Ramp basin through the tributary valley on the west shore of the lake rather than from the southwest end of the Tsunami Ramp basin (Fig. 2). Such an inundation route would lengthen the distance that tsunamis would need to travel to deposit sand in the basin by 500 m, and the <50 m width of the tributary valley would have restricted tsunami inflow. If relative sea level at Southwest Anchorage was >2 m lower than it is now during parts of Southwest Anchorage's history, bedrock platforms on its west side not far below MLLW may have also slowed the progress of inland-directed tsunamis. In contrast, the low dunes backing the beach on the southeast side of Southwest Anchorage would provide minimal resistance to high incoming tsunamis directed into Drained Lake basin. At the Drained Lake site, once tsunamis reached the apex of the gently sloping fan in the southwest facing valley, the steep, narrowing side slopes of the valley would have concentrated tsunami flows, allowing them to inundate farther up the valley.

The small number of pre–4 ka probable (4) and possible (4) tsunami deposits identified at the Tsunami Ramp site probably reflects the period 10–4 ka, when we infer relative sea level to have been considerably lower than present. The diamicton that we infer to be till at the base of Tsunami Ramp cores suggests that Chirikof Island may have had a relative sea-level history similar to ice-marginal sites on the Atlantic coast of North America, such as Maine, where modeled relative sea-level curves have a nonmonotonic form (e.g., Kelley et al., 2010; Engelhart et al., 2011). Such a curve with relative sea level within a few meters of its present level ca. 10.5 ka and from 4 ka to present is consistent with the distinct characteristics of the thick tsunami deposit at this site (bed C'; Table 2; Figs. 6 and 7; Fig. S3 in the Supplemental File [see footnote 1]). Thus, pre–4 ka stratigraphy provides little information about the recurrence of high tsunamis at Southwest Anchorage.

TSUNAMI RECURRENCE

Our grouping of tsunami deposits into probable and possible categories allows only maximum and minimum estimates of the recurrence of high tsunamis on Chirikof Island's southwest coast (Fig. 11). During the past 3500 yr at the Drained Lake site, tsunamis exceeding 5 m in height (above present MLLW) may have been as frequent as every 180 yr (both possible and probable in Table 2). Considering only probable tsunami deposits for the same period gives a late Holocene average of ~270 yr (Fig. 11). The presence of deposits of only four probable and two possible tsunamis at the Tsunami Ramp site (Table 1), all predating the late Holocene, makes its record too incomplete to be useful in estimating recurrence.

Elsewhere in the eastern Alaska-Aleutian arc, information on the recurrence of high tsunamis or the great earthquakes likely to have accompanied them over the past 3500 yr is limited (Carver and Plafker, 2008; Shennan et al., 2014a, 2014b; Kelsey et al., 2015). Carver and Plafker (2008) compiled radiocarbon ages from studies of Kodiak Island coastal stratigraphy by Carver and Gilpin (1992), Gilpin et al. (1994), and Gilpin (1995) to infer the times of four megathrust earthquakes prior to the 1964 earthquake, at least three of which were accompanied by tsunamis (Fig. 12). Shennan et al. (2014b) use diatom analysis of tidal stratigraphy to identify subsidence followed by a tsunami during the 1788 earthquake at four estuaries in northeastern Kodiak Island. Similar evidence at other sites led them to infer rupture of the Kodiak segment of the megathrust ca. A.D. 1440–1620 and ca. A.D. 1020–1150, times that do not overlap age distributions for probable tsunamis on Chirikof Island (Fig. 12). From stratigraphic and landform evidence on the Kenai Peninsula, 500 km northeast of Chirikof Island, Kelsey et al. (2015) inferred that the ca. A.D. 1020–1150 earthquake probably ruptured the Kenai Peninsula part of the megathrust, as suggested by Shennan et al. (2014a), and that a younger Kenai megathrust earthquake may have coincided with either the A.D. 1440–1620 or 1788 earthquakes. On Sitkalidak Island on the southeast coast of Kodiak Island, Mahrt (2006) interpreted two broadly dated sand beds extending 400 m inland as probable tsunami deposits. Hutchinson and Crowell (2007) suggested that six episodes of village abandonment, inferred from archaeological stratigraphy throughout the region, may have been caused by subsidence or tsunamis accompanying great earthquakes. Approximately 250 km west of Chirikof Island, Witter et al. (2014) could not find clear evidence of any high tsunamis in the past 3000 yr, despite Russian accounts of severe flooding during the 1788 tsunami.

On the south coast of Sitkinak Island, only 125 km east of Chirikof Island, Briggs et al. (2014a) identified uplift and subsidence during 5 great earthquakes and 6 possible tsunami beds dating from the past 3000 yr. The youngest of the beds, probably deposited by the 1788 tsunami, can be traced continuously 1.3 km inland. Five older sand beds with similar characteristics extend >0.8 km inland. Applying the methods that we used to construct the age distributions of Figure 11 to the ages reported by Briggs et al. (2014a), we calculate age distributions for the five older possible tsunami deposits on Sitkinak Island (Fig. 12). Comparing these distributions with those from Chirikof Island suggests that the same tsunamis may have inundated both islands ca. 2.4 ka, 2.3 ka, 2.0 ka, and 1.2 ka. No Chirikof Island correlative is available, however, for the 0.9–0.6 ka tsunami deposit at Sitkinak Island, which may have been deposited by the tsunami accompanying the ca. A.D. 1020–1150 earthquake on Kodiak Island (Fig. 12). The almost continuous overlap in the Chirikof Island age

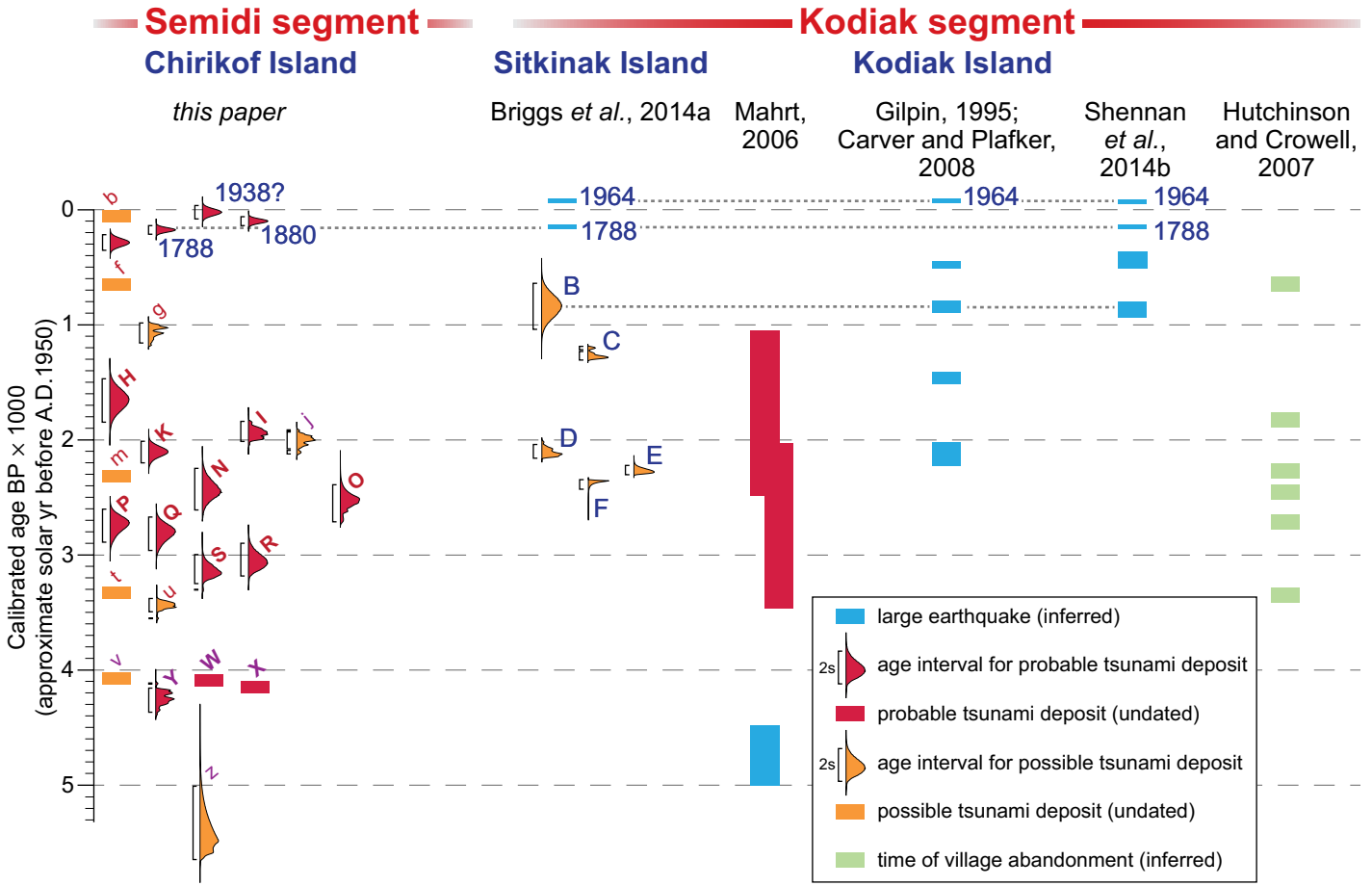

Figure 12. Age probability distributions for probable (red) and possible (orange) tsunami deposits at Southwest Anchorage (labels as in Fig. 11) compared with age distributions for possible tsunami deposits at Sitkinak Island (Briggs et al., 2014a) and with age estimates for great earthquakes and tsunamis on Kodiak Island (from studies referenced on this figure; Fig. 1). Dotted horizontal lines show our correlation of evidence for some younger earthquakes and tsunamis. Times of great earthquakes inferred from episodes of village abandonment determined from archaeological stratigraphy in the eastern Alaska-Aleutian megathrust region are also shown (Hutchinson and Crowell, 2007). Deposit labels as in Tables 1 and 2.

distributions between 3.5 ka and 1.5 ka permits a correlation with deposits of any age within this period.

What proportion of potential tsunami beds on Chirikof Island was deposited by tsunamis generated during upper plate faulting or submarine landslides near Chirikof Island independent of megathrust ruptures? Strong shaking may destabilize submarine slope deposits to produce a high tsunami (e.g., Okal et al., 2003; Fryer et al., 2004; Miller et al., 2014). Although Chirikof Island is more than 160 km from active volcanoes, submarine slides and volcanic debris avalanches have the potential to produce damaging transpacific tsunamis, which could reach 20 m on near-source Aleutian coasts (Waythomas et al., 2009). Waythomas et al. (2009) estimated a recurrence for >10-m-high tsunamis of this type as 2000 yr over the entire Aleutian arc, making it unlikely that any of the possible tsunami deposits in core D8 were deposited by a landslide-generated tsunami independent of a megathrust earthquake.

Historical accounts suggest that upper plate faulting during the 1880 earthquake produced a Chirikof Island tsunami, which we infer deposited bed C. Approximately 600 km to the northeast of Chirikof Island, Liberty et al. (2013) identified an area of mostly submarine upper plate faults with high rates of

slip that splay off the megathrust where it is most strongly coupled. Although each splay fault may rupture independently of the megathrust, following similar conclusions about analogous subduction zones (e.g., Melnick et al., 2006; Strasser et al., 2009) Liberty et al. (2013) argued that most splay faults slip during megathrust earthquakes and that the location of the area of high seismic coupling has changed little during the Holocene. Less is known about the complex structure of upper plate faults in Miocene and older shelf rocks near Chirikof Island (e.g., Lewis et al., 1988; von Huene et al., 2012), the complex upper plate structure of which may have played a role in halting the 1964 rupture (von Huene et al., 2012). Arc-vergent thrusts in these high-seismic-velocity continental rocks near Chirikof Island are probably capable of storing considerable strain and so are unlikely to slip independent of the megathrust (e.g., Cubas et al., 2013); the 1880 earthquake is an apparent exception. Normal faults reflecting extension near the slope, like those imaged in similar positions to the northeast and southwest (von Huene et al., 2012; Miller et al., 2014), would be too short to generate large earthquakes. Thus, we infer that no more than 2–3 of the 19 potential tsunami deposits in core D8 were caused by upper plate faulting or submarine landslides independent of great megathrust earthquakes.

Whether a tsunami inundates and deposits identifiable sediment at a particular site is dependent on many factors besides the dimensions of seafloor deformation during faulting. The variable source characteristics and tsunami-generating potential of megathrust ruptures in the region (Ryan et al., 2012b; Briggs et al., 2014a, 2014b; Shennan et al., 2014a, 2014b; Witter et al., 2014) suggest that Southwest Anchorage has been exposed to a large range in inundation heights that may only loosely correlate with tsunami volume, rupture extent, and earthquake magnitude. For this reason, forecasting future great earthquakes in the eastern Aleutian arc accompanied by southward-directed high tsunamis will require carefully reconstructed histories of rupture lengths and inundation extents for the past 3–5 k.y. at many sites (Ryan et al., 2012b). Until more complete tsunami chronologies are available, we recommend that a high-tsunami recurrence of ~180–270 yr (Fig. 11; 13–19 deposits in 3500 yr) be used in assessing the hazard from the Semidi segment of the eastern Aleutian arc.

ACKNOWLEDGMENTS

This work was supported by the Earthquake Hazards Program, the Coastal and Marine Geology Program, and the Multi-hazards Demonstration Project of the U.S. Geological Survey. Diatom studies by Dura were supported by the Institute of Marine and Coastal Science, Rutgers University, Academy of Natural Sciences, Philadelphia, and the Department of Earth and Environmental Science, University of Pennsylvania. Analyses by Engelhart were supported by the U.S. Department of Agriculture National Institute of Food and Agriculture, Hatch funding, and the Rhode Island Agricultural Experiment Station (contribution 5423). Geochemical analyses by Vane were supported by the British Geological Survey; Vane publishes with the permission of the Executive Director of the British Geological Survey. We thank the Alaska Maritime National Wildlife Refuge for permission to investigate Chirikof Island. Our pilots, Steve Harvey and Rolan Ruoss, made this research possible. Peter Haeussler, Steve Kirby, Holly Ryan, and Stephanie Ross were enthusiastic supporters and arranged funding. Deborah Carver and Gary Carver provided long-term accommodation and advice. Steve Angster and Lauralee Bossen helped with core studies and historical air photograph analysis. Ralph Wright told us about living on Chirikof Island in the early 1960s, and Donald W. Clark, Patrick Saltonstall, and Amy Steffian provided extensive unpublished information, including three unpublished reports and photographs from 1963 to 2013. An unpublished manuscript by L.T. Black, D.W. Clark, and K. Arndt (dated 21 September 2002; provided by D.W. Clark, October 2013) was invaluable for our interpretation of historical tsunamis. This paper was improved through comments by Rob Witter, Yuki Sawai, Adam Switzer, and an anonymous reviewer. Any use of trade, product, or firm names is for descriptive purposes only and does not imply endorsement by the U.S. Government.

REFERENCES CITED

Allan, J.C., and Komar, P.D., 2006, Climate controls on US west coast erosion processes: Journal of Coastal Research, v. 22, p. 511–529, doi:10.2112/03-0108.1.

Apotsos, A., Gelfenbaum, G., Jaffe, B., Watt, S., Peck, B., Buckley, M., and Stevens, A., 2011, Tsunami inundation and sediment transport in a sediment-limited embayment on American Samoa: Earth-Science Reviews, v. 107, p. 1–11, doi:10.1016/j.earscirev.2010.11.001.

Atwater, B.F., and Hemphill-Haley, E., 1997, Recurrence intervals for great earthquakes of the past 3,500 years at northeastern Willapa Bay, Washington: U.S. Geological Survey Professional Paper 1576, 108 p.

Ballantyne, C.K., and Whittington, G., 1987, Niveo-aeolian sand deposits on an Teallach, Wester Ross, Scotland: Royal Society of Edinburgh Transactions, Earth Sciences, v. 78, p. 51–63, doi:10.1017/S0263593300010956.

Barnes, P.M., Bostock, H.C., Neil, H.I., Strachan, L.J., and Gosling, M., 2013, A 2300-year record of the southern Alpine fault and Fiordland subduction zone, New Zealand, based on stacked turbidites: Seismological Society of America Bulletin, v. 103, p. 2424–2446, doi:10.1785/0120120314.

Berryman, K., Cooper, A., Norris, R., Villamor, P., Sutherland, R., Wright, T., Schermer, E., Langridge, R., and Biasi, G., 2012, Late Holocene rupture history of the Alpine fault in South Westland, New Zealand: Seismological Society of America Bulletin, v. 102, p. 620–638, doi:10.1785/0120110177.

Bourgeois, J., 2009, Geologic effects and records of tsunamis, *in* Bernard, E.N., and Robinson, A.R., eds., Tsunamis: The Sea, Volume 15: Cambridge, USA, Harvard University Press, p. 55–91.

Bourgeois, J., Pinegina, T.K., Ponomareva, V., and Zaretskaia, N., 2006, Holocene tsunamis in the southwestern Bering Sea, Russian Far East, and their tectonic implications: Geological Society of America Bulletin, v. 118, p. 449–463, doi:10.1130/B25726.1.

Brain, M.J., Long, A.J., Petley, D.N., Horton, B.P., and Allison, R.J., 2011, Compression behaviour of minerogenic low energy intertidal sediments: Sedimentary Geology, v. 233, p. 28–41, doi:10.1016/j.sedgeo.2010.10.005.

Briggs, R.W., et al., 2006, Deformation and slip along the Sunda megathrust in the great 2005 Nias-Simeulue earthquake: Science, v. 311, no. 5769, p. 1897–1901, doi:10.1126/science.1122602.

Briggs, R.W., Engelhart, S.E., Nelson, A.R., Dura, T., Kemp, A.C., Haeussler, P.J., Corbett, D.R., Angster, S.J., and Bradley, L.-A., 2014a, Uplift and subsidence reveal a non-persistent megathrust rupture boundary, Sitkinak Island, Alaska: Geophysical Research Letters, v. 41, p. 2289–2296, doi:10.1002/2014GL059380.

Briggs, R.W., Witter, R.C., Nelson, A.R., Koehler, R.D., Haeussler, P.J., Engelhart, S.E., Gelfenbaum G., Dura, T., and Carver, G., 2014b, Implications of recent paleoseismic observations for models of Alaska-Aleutian megathrust rupture [abs.]: Seismological Research Letters, v. 85, p. 474.

Brill, D., Klasen, N., Jankaew, K., Brückner, H., Kelletat, D., Scheffers, A., and Scheffers, S., 2012, Local inundation distances and regional tsunami recurrence in the Indian Ocean inferred from luminescence dating of sandy deposits in Thailand: Natural Hazards Earth System Science, v. 12, no. 7, p. 2177–2192, doi:10.5194/nhess-12-2177-2012.

Bronk Ramsey, C., 2008, Depositional models for chronological records: Quaternary Science Reviews, v. 27, p. 42–60, doi:10.1016/j.quascirev.2007.01.019.

Bronk Ramsey, C., 2009, Bayesian analysis of radiocarbon dates: Radiocarbon, v. 51, p. 337–360.

Brugam, R.B., and Swain, P., 2000, Diatom indicators of peatland development at Pogonia Bog Pond, Minnesota, USA: The Holocene, v. 10, p. 453–464, doi:10.1191/095968300668251084.

Butler, R., 2012, Re-examination of the potential for great earthquakes along the Aleutian Island Arc with implications for tsunamis in Hawaii: Seismological Research Letters, v. 83, p. 29–38, doi:10.1785/gssrl.83.1.29.

Butler, R., Burney, D., and Walsh, D., 2014, Paleotsunami evidence on Kaua'i and numerical modeling of a great Aleutian tsunami: Geophysical Research Letters, v. 41, p. 6795–6802, doi:10.1002/2014GL061232.

Carver, G., and Gilpin, I.M., 1992, Paleoseismicity of Kodiak Island, Alaska, *in* Jacobson, M.L., compiler, National Earthquake Hazards Reduction Program, summaries of technical reports; Volume XXXIII: U.S. Geological Survey Open-File Report 92-258, p. 192–194.

Carver, G., and Plafker, G., 2008, Paleoseismicity and neotectonics of the Aleutian subduction zone, *in* Freymueller, J.T., et al., eds., Active tectonics and seismic potential of Alaska: American Geophysical Union Geophysical Monograph 179, p. 43–63, doi:10.1029/179GM03.

Chaffin, Y.M., 1967, Koniag to King Crab: Kodiak, Alaska, Chaffin Inc., 247 p.

Chaffin, Y.M., Krieger, T.H., and Rostad, M., 1983, Alaska's Konyag Country: Kodiak, Alaska, Chaffin Inc., 269 p.

Chagué-Goff, C., 2010, Chemical signatures of palaeotsunamis: A forgotten proxy?: Marine Geology, v. 271, p. 67–71, doi:10.1016/j.margeo.2010.01.010.

Chagué-Goff, C., and Goff, J.R., 1999, Geochemical and sedimentological signature of catastrophic saltwater inundations (tsunami), New Zealand: Quaternary Australasia, v. 17, p. 38–48.

Chagué-Goff, C., Schneider, J.-L., Goff, J.R., Dominey-Howes, D., and Strotz, L., 2011, Expanding the proxy tool kit to help identify past events—Lessons from the 2004 Indian Ocean tsunami and the 2009 South Pacific tsunami: Earth-Science Reviews, v. 107, p. 107–122, doi:10.1016/j.earscirev.2011.03.007.

Chagué-Goff, C., et al., 2012, Multi-proxy evidence for trans-Pacific tsunamis in the Hawai'ian Islands: Marine Geology, v. 299–302, p. 77–89, doi:10.1016/j.margeo.2011.12.010.

Chagué-Goff, C., Goff, J., Wong, H.K.Y., and Cisternas, M., 2015, Insights from geochemistry and diatoms to characterize a tsunami's deposit and maximum inundation limit: Marine Geology, v. 359, p. 22–34, doi:10.1016/j.margeo.2014.11.009.

Charles, D.F., Knowles, C., and Davis, R.S., eds., 2002, Protocols for the analysis of algal samples collected as part of the U.S. Geological Survey National Water-Quality Assessment program: Philadelphia, Pennsylvania, Academy of Natural Sciences Report 02–06, 132 p.

Cisternas, M., et al., 2005, Predecessors to the giant 1960 Chile earthquake: Nature, v. 437, no. 7057, p. 404–407, doi:10.1038/nature03943.

Clague, J.J., Wohlfarth, B., Ayotte, J., Eriksson, M., Hutchinson, I., Mathewes, R.W., and Walker, L., 2004, Late Holocene environmental change at treeline in the northern Coast Mountains, British Columbia, Canada: Quaternary Science Reviews, v. 23, p. 2413–2431, doi:10.1016/j.quascirev.2004.01.009.

Clark, D.W., 2010, Ground squirrel: The mysterious rodent of Kodiak: Arctic Anthropology, v. 47, p. 59–68, doi:10.1353/arc.2010.0005.

Coghlan, A., 2013, A little book of R for multivariate analysis: Cambridge, UK, Wellcome Trust Sanger Institute, 51 p.: https://media.readthedocs.org/pdf/little-book-of-r-for-multivariate-analysis/latest/little-book-of-r-for-multivariate-analysis.pdf.

Cohee, G.V., Bates, R.G., and Wright, W.B., 1969, Changes in stratigraphic nomenclature by the U.S. Geological Survey, 1969—Contributions to stratigraphy: U.S. Geological Survey Bulletin 1274-A, 41 p.

Cooper, S., Gaiser, E., and Wachnicka, A., 2010, Estuarine paleoenvironmental reconstructions using diatoms, *in* Smol, J.P., and Stoermer, E.F., eds., The diatoms: Applications for the environmental and earth sciences (second edition): Cambridge, U.K., Cambridge University Press, p. 324–345, doi:10.1017/CBO9780511763175.

Crawford, R.M., Likhoshway, Y.V., and Jahn, R., 2003, Morphology and identity of *Aulacoseira italica* and typification of *Aulacoseira* (Bacillariophyta): Diatom Research, v. 18, p. 1–19, doi:10.1080/0269249X.2003.9705569.

Cubas, N., Avouac, J.-P., Souloumiac, P., and Leroy, Y., 2013, Megathrust friction determined from mechanical analysis of the forearc in the Maule earthquake area: Earth and Planetary Science Letters, v. 381, p. 92–103, doi:10.1016/j.epsl.2013.07.037.

Davies, J., Sykes, L., House, L., and Jacob, K., 1981, Shumagin seismic gap, Alaska Peninsula: History of great earthquakes, tectonic setting, and evidence for high seismic potential: Journal of Geophysical Research, v. 86, no. B5, p. 3821–3855, doi:10.1029/JB086iB05p03821.

Davies, M.H., Mix, A.C., Stoner, J.S., Addison, J.A., Jaeger, J., Finney, B., and Wiest, J., 2011, The deglacial transition on the southeastern Alaska Margin: Meltwater input, sea level rise, marine productivity, and sedimentary anoxia: Paleoceanography, v. 26, PA2223, doi:10.1029/2010PA002051.

Dawson, A.G., and Shi, S., 2000, Tsunami deposits: Pure and Applied Geophysics, v. 157, p. 875–897, doi:10.1007/s000240050010.

Dawson, A.G., and Stewart, I., 2007, Tsunami deposits in the geological record: Sedimentary Geology, v. 200, p. 166–183, doi:10.1016/j.sedgeo.2007.01.002.

Dawson, A.G., Foster, I.D.L., Shi, S., Smith, D.E., and Long, D., 1991, The identification of tsunami deposits in coastal sediment sequences: Science of Tsunami Hazards, v. 9, p. 73–82.

Dawson, S., 2007, Diatom biostratigraphy of tsunami deposits: Examples from the 1998 Papua New Guinea tsunami: Sedimentary Geology, v. 200, p. 328–335, doi:10.1016/j.sedgeo.2007.01.011.

Dawson, S., and Smith, D.E., 2000, The sedimentology of Middle Holocene tsunami facies in northern Sutherland, Scotland, UK: Marine Geology, v. 170, p. 69–79, doi:10.1016/S0025-3227(00)00066-9.

Dawson, S., Smith, D.E., Ruffman, A., and Shi, S., 1996, The diatom biostratigraphy of tsunami sediments: Examples from recent and middle Holocene events: Physics and Chemistry of the Earth, v. 21, p. 87–92, doi:10.1016/S0079-1946(97)00015-3.

Denys, L., 1991, A checklist of the diatoms in the Holocene deposits of the western Belgian coastal plain with a survey of their apparent ecological requirements I: Introduction, ecological code and complete list: Ministère des affaires économiques, Service Géologique de Belgique, Professional Paper 246, 41 p

Dominey-Howes, D.T.M., Humphreys, G.S., and Hesse, P.P., 2006, Tsunami and palaeotsunami depositional signatures and their potential value in understanding the late-Holocene tsunami record: The Holocene, v. 16, p. 1095–1107, doi:10.1177/0959683606069400.

DuRoss, C.B., Personius, S.F., Crone, A.J., Olig, S.S., and Lund, W.R., 2011, Integration of paleoseismic data from multiple sites to develop an objective earthquake chronology: Application to the Weber segment of the Wasatch fault zone, Utah: Seismological Society of America Bulletin, v. 101, p. 2765–2781, doi:10.1785/0120110102.

Engelhart, S.E., Horton, B.P., and Kemp, A.C., 2011, Holocene sea level changes along the United States' Atlantic coast: Oceanography, v. 24, p. 70–79, doi:10.5670/oceanog.2011.28.

Estabrook, C.H., Jacob, K.H., and Sykes, L.R., 1994, Body wave and surface wave analysis of large and great earthquakes along the Eastern Aleutian Arc, 1923–1993: Implications for future event: Journal of Geophysical Research, v. 99, no. B6, p. 11,643–11,662, doi:10.1029/93JB03124.

Fields, W.M., 2000, Now it can be told: Stories of Alaskan pioneer ranchers: Anchorage, Alaska, Publications Consultants, 311 p.

Folk, R.L., and Ward, W.C., 1957, Brazos river bar: A study in the significance of grain size parameters: Journal of Sedimentary Petrology, v. 27, p. 3–26, doi:10.1306/74D70646-2B21-11D7-8648000102C1865D.

Fournier, T.J., and Freymueller, J.T., 2007, Transition from locked to creeping subduction in the Shumagin region, Alaska: Geophysical Research Letters, v. 34, L06303, doi:10.1029/2006GL029073.

Freymueller, J.T., Woodard, H., Cohen, S.C., Cross, R., Elliot, J., Larsen, C.F., Hreinsdóttir, S., and Zweck, C., 2008, Active deformation processes in Alaska, based on 15 years of GPS measurements, *in* Freymueller, J.T., et al., eds., Active tectonics and seismic potential of Alaska: American Geophysical Union Geophysical Monograph Series 179, p. 1–42, doi:10.1029/179GM02.

Fryer, G.J., Watts, P., and Pratson, L.F., 2004, Source of the great tsunami of 1 April 1946: A landslide in the upper Aleutian forearc: Marine Geology, v. 203, p. 201–218, doi:10.1016/S0025-3227(03)00305-0.

Gelfenbaum, G., and Jaffe, B., 2003, Erosion and sedimentation from the 17 July, 1998 Papua New Guinea tsunami: Pure and Applied Geophysics, v. 160, p. 1969–1999, doi:10.1007/s00024-003-2416-y.

Gilpin, L.M., 1995, Holocene paleoseismicity and coastal tectonics of the Kodiak Islands, Alaska [Ph.D. thesis]: Santa Cruz, University of California, 358 p.

Gilpin, L.M., Ward, S., Anderson, R., Moore, J.C., and Carver, G.A., 1994, Holocene interseismic deformation and stratigraphic modeling of the earthquake cycle, Kodiak Islands, Alaska: U.S. Geological Survey Open-File Report 94-176, p. 339–344.

Goff, J., McFadgen, B.G., and Chagué-Goff, C., 2004, Sedimentary differences between the 2002 Easter storm and the 15th-century Okoropunga tsunami, southeastern North Island, New Zealand: Marine Geology, v. 204, p. 235–250, doi:10.1016/S0025-3227(03)00352-9.

Goff, J., Pearce, S., Nichol, S., Chagué-Goff, C., Horrocks, M., and Strotz, L., 2010, Multi-proxy records of regionally-sourced tsunamis, New Zealand: Geomorphology, v. 118, p. 369–382, doi:10.1016/j.geomorph.2010.02.005.

Goff, J., Chagué-Goff, C., Nichol, S., Jaffe, B., and Dominey-Howes, D., 2012, Progress in palaeotsunami research: Sedimentary Geology, v. 243–244, p. 70–88, doi:10.1016/j.sedgeo.2011.11.002.

Goldfinger, C., et al., 2012, Turbidite event history: Methods and implications for Holocene paleoseismicity of the Cascadia subduction zone: U.S. Geological Survey Professional Paper 1661-F, 332 p.

Goto, K., et al., 2011, New insights of tsunami hazard from the 2011 Tohoku-Oki event: Marine Geology, v. 290, p. 46–50, doi:10.1016/j.margeo.2011.10.004.

Hartley, B., Barber, H.G., Carter, J.R., and Sims, P.A., 1996, An atlas of British diatoms: Bristol, UK, Biopress, 601 p.

Hemphill-Haley, E., 1995, Diatoms evidence for earthquake-induced subsidence and tsunami 300 yr ago in southern coastal Washington: Geological Society of America Bulletin, v. 107, p. 367–378, doi:10.1130/0016-7606(1995)107<0367:DEFEIS>2.3.CO;2.

Hemphill-Haley, E., 1996, Diatoms as an aid in identifying late Holocene tsunami deposits: The Holocene, v. 6, p. 439–448, doi:10.1177/095968369600600406.

Hutchinson, I., and Crowell, A.L., 2007, Recurrence and extent of great earthquakes in southern Alaska during the late Holocene from an analysis of the radiocarbon record of land-level change and village abandonment: Radiocarbon, v. 49, p. 1323–1385.

Hutchinson, I., Clague, J.J., and Mathewes, R.W., 1997, Reconstructing the tsunami record on an emerging coast: A case study of Kanim Lake, Vancouver Island, British Columbia, Canada: Journal of Coastal Research, v. 13, p. 545–553.

Jaffe, B.E., Goto, K., Sugawara, D., Richmond, B., Fujino, S., and Nishimura, Y., 2012, Flow speed estimated by inverse modelling of sandy tsunami deposits: Results from the 11 March 2011 tsunami on the coastal plain near the Sendai Airport, Honshu, Japan: Sedimentary Geology, v. 282, p. 90–109, doi:10.1016/j.sedgeo.2012.09.002.

Jankaew, K., Atwater, B.F., Sawai, Y., Choowong, M., Charoentitirat, T., Martin, M.E., and Prendergast, A., 2008, Medieval forewarning of the 2004 Indian Ocean tsunami in Thailand: Nature, v. 455, p. 1228–1231, doi:10.1038/nature07373.

Johnson, J.M., and Satake, K., 1994, Rupture extent of the 1938 Alaskan earthquake as inferred from tsunami waveforms: Geophysical Research Letters, v. 21, p. 733–736, doi:10.1029/94GL00333.

Keithahn, E.L., 1962, Chirikof, the foggy island: Alaska Sportsman, v. 28, no. 4, p. 16–17.

Kelley, J.T., Belknap, D.F., and Claesson, S., 2010, Drowned coastal deposits with associated archaeological remains from a sea-level "slowstand": Northwestern Gulf of Maine: Geology, v. 38, p. 695–698, doi:10.1130/G31002.1.

Kelsey, H.M., Nelson, A.R., Hemphill-Haley, E., and Witter, R.C., 2005, Tsunami history of an Oregon coastal lake reveals a 4600 yr record of great earthquakes on the Cascadia subduction zone: Geological Society of America Bulletin, v. 117, p. 1009–1032, doi:10.1130/B25452.1.

Kelsey, H.M., Witter, R.C., Engelhart, S.E., Briggs, R.W., Nelson, A.R., Haeussler, P.J., and Corbett, D.R., 2015, Beach ridges as paleoseismic indicators of abrupt coastal subsidence during subduction zone earthquakes, and implications for Alaska-Aleutian subduction zone paleoseismology, southeast coast of the Kenai Peninsula, Alaska: Quaternary Science Reviews, v. 113, p. 147–158, doi:10.1016/j.quascirev.2015.01.006.

Kemp, A.C., Horton, B.P., Vane, C.H., Bernhardt, C.E., Reide Corbett, D., Engelhart, S.E., Anisfeld, S.C., Parnell, A.C., and Cahill, N., 2013, Sea-level change during the last 2500 years in New Jersey, USA: Quaternary Science Reviews, v. 81, p. 90–104, doi:10.1016/j.quascirev.2013.09.024.

Knell, R., 2013, Introductory R: A beginner's guide to data visualisation, statistical analysis and programming in R: Walton on Thames, UK, Hersham, 531 p.

Kokociński, M., Szczuciński, W., Zgrundo, A., and Ibragimow, A., 2009, Diatom assemblages in 26 December 2004 tsunami deposits from coastal zone of Thailand as sediment provenance indicators: Polish Journal of Environmental Studies, v. 18, p. 93–101.

Kortekaas, S., and Dawson, A.G., 2007, Distinguishing tsunami and storm deposits: An example from Martinhal, SW Portugal: Sedimentary Geology, v. 200, p. 208–221, doi:10.1016/j.sedgeo.2007.01.004.

Koster, E.A., and Dijkmans, J.W.A., 1988, Niveo-aeolian deposits and denivation forms, with special reference to the Great Kobuk sand dunes, northwestern Alaska: Earth Surface Processes and Landforms, v. 13, p. 153–170, doi:10.1002/esp.3290130206.

Krammer, K., and Lange-Bertalot, H., 1986, *Bacillarophyceae* 1. Teil *Naviculaceae*: Süßwasserflora von Mitteleuropa, Band 2/1: Stuttgart, Gustav Fischer Verlag, 876 p.

Krammer, K., and Lange-Bertalot, H., 1988, *Bacillarophyceae* 2. Teil *Basillariaceae*, *Epithemiaceae*, *Surirellaceae*: Süßwasserflora von Mitteleuropa Band 2/2: Stuttgart, Gustav Fischer Verlag, 600 p.

Krammer, K., and Lange-Bertalot, H., 1991a, *Bacillarophyceae* 3. Teil *Centrales*, *Fragilariaceae*, *Eunotiaceae*: Süßwasserflora von Mitteleuropa Band 2/3: Stuttgart, Gustav Fischer Verlag, 600 p.

Krammer, K., and Lange-Bertalot, H., 1991b, *Bacillarophyceae* 4. *Achnanthaceae*, *Kritische Erganzungen zu Navicula (Lineolatae)* und *Gomphonema*: Süßwasserflora von Mitteleuropa Band 2/4: Stuttgart, Gustav Fischer Verlag, 437 p.

Lander, J.F., 1996, Tsunamis affecting Alaska 1737–1996: Boulder, Colorado, National Geographic Data Center, NGDC Key to Geophysical Research Documentation no. 31, 195 p.

Lander, J.F., and Lockridge, P.A., 1989, United States tsunamis (including United States possessions), 1690–1988: Boulder, Colorado, National Geographic Data Center, NGDC Publication 41-2, 265 p.

Lewis, S.D., Ladd, J.W., and Bruns, T.R., 1988, Structural development of an accretionary prism by thrust and strike-slip faulting: Shumagin region, Aleutian Trench: Geological Society of America Bulletin, v. 100, p. 767–782, doi:10.1130/0016-7606(1988)100<0767:SDOAAP>2.3.CO;2.

Liberty, L.M., Finn, S.P., Haeussler, P.J., Pratt, T.L., and Peterson, A., 2013, Megathrust splay faults at the focus of the Prince William Sound asperity, Alaska: Journal of Geophysical Research, v. 118, p. 5428–5441, doi:10.1002/jgrb.50372.

Lienkaemper, J.J., and Bronk Ramsey, C., 2009, OxCal: Versatile tool for developing paleoearthquake chronologies—A primer: Seismological Research Letters, v. 80, p. 431–434, doi:10.1785/gssrl.80.3.431.

Long, J.S., 1975, McCord of Alaska: Statesman for the last frontier: Cleveland, Ohio, Dillon/Liederbach, Inc., 210 p.

López, A.M., and Okal, E.A., 2006, A seismological reassessment of the source of the 1946 Aleutian "tsunami" earthquake: Geophysical Journal International, v. 165, p. 835–849, doi:10.1111/j.1365-246X.2006.02899.x.

MacInnes, B.T., Bourgeois, J., Pinegina, T.K., and Kravchunovskaya, E.A., 2009, Tsunami geomorphology: Erosion and deposition from the 15 November 2006 Kuril Island tsunami: Geology, v. 37, p. 995–998, doi:10.1130/G30172A.1.

MacNeil, M.D., Cronin, M.A., Blackburn, H.D., Richards, C.M., Lockwood, D.R., and Alexander, L.J., 2007, Genetic relationships between feral cattle from Chirikof Island, Alaska and other breeds: Animal Genetics, v. 38, p. 193–197, doi:10.1111/j.1365-2052.2007.01559.x.

Mahrt, E., 2006, Rise and fall in Tanginak Anchorage, Sitkalidak Island, Alaska: A Holocene geologic history [M.S. thesis]: Seattle, University of Washington, 126 p.

McCaffrey, R., 2008, Global frequency of magnitude 9 earthquakes: Geology, v. 36, p. 263–266, doi:10.1130/G24402A.1.

Melnick, D., Bookhagen, B., Echtler, H., and Strecker, M.R., 2006, Coastal deformation and great subduction earthquakes, Isla Santa María, Chile (37°S): Geological Society of America Bulletin, v. 118, p. 1463–1480, doi:10.1130/B25865.1.

Melnick, D., Moreno, M., Motagh, M., Cisternas, M., and Wesson, R.L., 2012, Splay fault slip during the M_w 8.8 2010 Maule Chile earthquake: Geology, v. 40, p. 251–254, doi:10.1130/G32712.1.

Miller, J.J., von Huene, R., and Ryan, H.F., 2014, The 1946 Unimak tsunami earthquake area—Revised tectonic structure in reprocessed seismic images and a suspect near field tsunami source: U.S. Geological Survey Open-File Report 2014-1024, 19 p., http://dx.doi.org/10.3133/ofr20141024.

Minoura, K., and Nakata, T., 1994, Discovery of an ancient tsunami deposit in coastal sequences of southwest Japan: Verification of a large historic tsunami: The Island Arc, v. 3, p. 66–72, doi:10.1111/j.1440-1738.1994.tb00006.x.

Minoura, K., and Nakaya, S., 1991, Traces of tsunami preserved in inter-tidal lacustrine and marsh deposits: Some examples from northeast Japan: Journal of Geology, v. 99, p. 265–287, doi:10.1086/629488.

Minoura, K., Imamura, F., Sugawara, D., Kono, Y., and Iwashita, T., 2001, The 869 Jogan tsunami deposit and recurrence interval of large-scale tsunami on the Pacific coast of northeast Japan: Journal of Natural Disaster Science, v. 23, p. 83–88.

Monecke, K., Finger, W., Klarer, D., Kongko, W., McAdoo, B.G., Moore, A.L., and Sudrajat, S.U., 2008, A 1,000-year sediment record of tsunami recurrence in northern Sumatra: Nature, v. 455, p. 1232–1234, doi:10.1038/nature07374.

Morton, R.A., Gelfenbaum, G., and Jaffe, B.E., 2007, Physical criteria for distinguishing sandy tsunami and storm deposits using modern examples: Sedimentary Geology, v. 200, p. 184–207, doi:10.1016/j.sedgeo.2007.01.003.

Murray, A.S., and Wintle, A.G., 2003, The single aliquot regenerative dose protocol: Potential for improvements in reliability: Radiation Measurements, v. 37, p. 377–381, doi:10.1016/S1350-4487(03)00053-2.

Nanayama, F., Shigeno, K., Satake, K., Shimokawa, K., Koitabashi, S., Miyasaka, S., and Ishii, M., 2000, Sedimentary differences between the 1993 Hokkaido-nansei-oki tsunami and the

1959 Miyakojima typhoon at Taisei, southwestern Hokkaido, northern Japan: Sedimentary Geology, v. 135, p. 255–264.
Nanayama, F., Satake, K., Furukawa, R., Shimokawa, K., Atwater, B.F., Shigeno, K., and Yamaki, S., 2003, Unusually large earthquakes inferred from tsunami deposits along the Kuril trench: Nature, v. 424, p. 660–663, doi:10.1038/nature01864.
Nanayama, F., Furukawa, R., Shigeno, K., Makino, A., Soeda, Y., and Igarashi, Y., 2007, Nine unusually large tsunami deposits from the past 4000 years at Kiritappu marsh along the southern Kuril Trench: Sedimentary Geology, v. 200, p. 275–294, doi:10.1016/j.sedgeo.2007.01.008.
Nelson, A.R., 2015, Coastal sediment, *in* Shennan, I., et al., eds., Handbook of sea-level research: Chichester, UK, Wiley-Blackwell, p. 218–272.
Nelson, A.R., Sawai, Y., Jennings, A.E., Bradley, L.-A., Gerson, L., Sherrod, B.L., Sabean, J., and Horton, B.J., 2008, Great-earthquake paleogeodesy and tsunamis of the past 2000 years at Alsea Bay, central Oregon coast, USA: Quaternary Science Reviews, v. 27, p. 747–768, doi:10.1016/j.quascirev.2008.01.001.
Nilsen, T.H., and Moore, G.W., 1979, Reconnaissance study of Upper Cretaceous to Miocene stratigraphic units and sedimentary facies, Kodiak and adjacent islands, Alaska, with a section on sedimentary petrography: U.S. Geological Survey Professional Paper 1093, 34 p., http://pubs.usgs.gov/pp/1093/report.pdf.
Nishenko, S.P., and Jacob, K.H., 1990, Seismic potential of the Queen Charlotte–Alaska–Aleutian seismic zone: Journal of Geophysical Research, v. 95, no. B3, p. 2511–2532, doi:10.1029/JB095iB03p02511.
Okal, E.A., Plafker, G., Synolakis, C.E., and Borrero, J.C., 2003, Near-field survey of the 1946 Aleutian tsunami on Unimak and Sanak Islands: Seismological Society of America Bulletin, v. 93, p. 1226–1234, doi:10.1785/0120020198.
Paul, C.A., Douglas, M.S.V., and Smol, J.P., 2010, Diatom-inferred Holocene climatic and environmental changes in an unusually subsaline high Arctic nunatak pond on Ellesmere Island (Nunavut, Canada): Journal of Paleolimnology, v. 44, p. 913–929, doi:10.1007/s10933-010-9464-y.
Peters, R., and Jaffe, B., 2010, Identification of tsunami deposits in the geologic record: Developing criteria using recent tsunami deposits: U.S. Geological Survey Open-File Report 2010–1239, 39 p.
Pierson, J., Forman, S.L., and Mazzocco, J., 2010, A residual-corrected cluster analysis for luminescence dating: Proceedings, New World Luminescence Dating Workshop, 7th, Montreal, Quebec, p. 14.
Pilarczyk, J.E., Horton, B.P., Witter, R.C., Vane, C.H., Chagué-Goff, C., and Goff, J., 2012, Sedimentary and foraminiferal evidence of the 2011 Tōhoku-Oki tsunami on the Sendai coastal plain, Japan: Sedimentary Geology, v. 282, p. 78–89, doi:10.1016/j.sedgeo.2012.08.011.
Plafker, G., and Kachadoorian, R., 1966, Geologic effects of the March 1964 earthquake and associated seismic sea waves on Kodiak and nearby islands, Alaska: U.S. Geological Survey Professional Paper 543-D, p. D1–D46.
Prendergast, A.L., Cupper, M.L., Jankaew, K., and Sawai, Y., 2012, Indian Ocean tsunami recurrence from optical dating of tsunami sand sheets in Thailand: Marine Geology, v. 295–298, p. 20–27, doi: 10.1016/j.margeo.2011.11.012.
Prescott, J.R., and Hutton, J.T., 1994, Cosmic ray contributions to dose rates for luminescence and ESR dating: Large depths and long-term time variations: Radiation Measurements, v. 23, p. 497–500, doi:10.1016/1350-4487(94)90086-8.
Ramírez-Herrera, M.-T., et al., 2012, Extreme wave deposits on the Pacific coast of Mexico: tsunamis or storms? A multi-proxy approach: Geomorphology, v. 139–140, p. 360–371, doi:10.1016/j.geomorph.2011.11.002.
Reimer, P.J., et al., 2013, IntCal13 and Marine13 radiocarbon age calibration curves 0–50,000 years cal BP: Radiocarbon, v. 55, p. 1869–1887, doi:10.2458/azu_js_rc.55.16947.
Ross, S.L., et al., 2013, The SAFRR (Science Application for Risk Reduction) tsunami scenario—Executive summary and introduction: U.S. Geological Survey Open-File Report 2013-1170-A, 17 p.
Rothwell, R.G., and Rack, F.R., 2006, New techniques in sediment core analysis: An introduction, *in* Rothwell, R.G., ed., New techniques in sediment core analysis: Geological Society of London Special Publication 267, p. 1–29, doi:10.1144/GSL.SP.2006.267.01.20.
Rühland, K., Smol, J.P., Jasinski, J.P., and Warner, B.G., 2000, Response of diatoms and other siliceous indicators to the developmental history of a peatland in the Tiksi Forest, Siberia, Russia: Arctic, Antarctic, and Alpine Research, v. 32, p. 167–178, doi:10.2307/1552448.
Ruppert, N.A., Lees, J.M., and Kozyreva, N.P., 2013, Seismicity, earthquakes and structure along the Alaska-Aleutian and Kamchatka-Kurile subduction zones: A review, *in* Eichelberger, J., et al., eds., Volcanism and subduction: The Kamchatka region: American Geophysical Union Geophysical Monograph 172, p. 129–144, doi:10.1029/172GM12.
Ryan, H., von Huene, R., Scholl, D., and Kirby, S., 2012a, Tsunami hazards to U.S. coasts from giant earthquakes in Alaska: Eos (Transactions, American Geophysical Union), v. 93, p. 185–192, doi:10.1029/2012EO190001.
Ryan, H.F., von Huene, R., Wells, R.E., Scholl, D.W., Kirby, S., and Draut, A.E., 2012b, History of earthquakes and tsunamis along the eastern Aleutian-Alaska megathrust, with implications for tsunami hazards in the California continental borderland, *in* Dumoulin, J.A., and Dusel-Bacon, C., eds., Studies by the U.S. Geological Survey in Alaska, 2011: U.S. Geological Survey Professional Paper 1795-A, 31 p.
Satake, K., 2014, Advances in earthquake and tsunami sciences and disaster risk reduction since the 2004 Indian Ocean tsunami: Geoscience Letters, v. 1, 15 p., doi:10.1186/s40562-014-0015-7.
Satake, K., and Atwater, B.F., 2007, Long-term perspectives on giant earthquakes and tsunamis at subduction zones: Annual Review of Earth and Planetary Sciences, v. 35, p. 349–374, doi:10.1146/annurev.earth.35.031306.140302.
Sauber, J., Carver, G., Cohen, S., and King, R., 2006, Crustal deformation and the seismic cycle across the Kodiak Islands, Alaska: Journal of Geophysical Research, v. 111, no. B2, B02403, doi:10.1029/2005JB003626.
Sawai, Y., 2002, Evidence for 17th-century tsunamis generated on the Kuril-Kamchatka subduction zone, Lake Tokotan, Hokkaido, Japan: Journal of Asian Earth Sciences, v. 20, p. 903–911, doi:10.1016/S1367-9120(01)00077-3.
Sawai, Y., Fujii, Y., Fujiwara, O., Kamataki, T., Komatsubara, J., Okamura, Y., Satake, K., and Shishikura, M., 2008, Marine incursions of the past 1500 years and evidence of tsunamis at Suijin-numa, a coastal lake facing the Japan Trench: The Holocene, v. 18, p. 517–528, doi:10.1177/0959683608089206.
Sawai, Y., Jankaew, K., Martin, M.E., Prendergast, A., Choowong, M., and Charoentitirat, T., 2009, Diatom assemblages in tsunami deposits associated with the 2004 Indian Ocean tsunami at Phra Thong Island, Thailand: Marine Micropaleontology, v. 73, p. 70–79, doi:10.1016/j.marmicro.2009.07.003.
Sawai, Y., Namegaya, Y., Okamura, Y., Satake, K., and Shishikura, M., 2012, Challenges of anticipating the 2011 Tohoku earthquake and tsunami using coastal geology: Geophysical Research Letters, v. 39, no. 21, doi:10.1029/2012GL053692.
Shennan, I., and Hamilton, S.L., 2006, Coseismic and pre-seismic subsidence associated with great earthquakes in Alaska: Quaternary Science Reviews, v. 25, p. 1–8, doi:10.1016/j.quascirev.2005.09.002.
Shennan, I., Long, A., and Barlow, N., 2007, Recurrent Holocene paleoseismicity and associated land/sea-level changes in south central Alaska (U.S. Geological Survey External Grant Award 06HQGR0033): Durham, UK, University of Durham, 39 p., http://earthquake.usgs.gov/research/external/reports/06HQGR0033.pdf.
Shennan, I., Bruhn, R., and Plafker, G., 2009, Multi-segment earthquakes and tsunami potential of the Aleutian megathrust: Quaternary Science Reviews, v. 28, p. 7–13, doi:10.1016/j.quascirev.2008.09.016.
Shennan, I., Long, A., Barlow, N., and Watcham, E., 2010, Spatial and temporal patterns of deformation associated with multiple late Holocene earthquakes in Alaska (U.S. Geological Survey External Grant Award G09AP00105): Durham, UK, University of Durham, 42 p., http://earthquake.usgs.gov/research/external/reports/G10AP00075.pdf.
Shennan, I., Bruhn, R., Barlow, N., Good, K., and Hocking, E., 2014a, Late Holocene great earthquakes in the eastern part of the Aleutian megathrust: Quaternary Science Reviews, v. 84, p. 86–97, doi:10.1016/j.quascirev.2013.11.010.
Shennan, I., Barlow, N., Carver, G., Davies, F., Garrett, E., and Hocking, E., 2014b, Great tsunamigenic earthquakes during the past 1000 yr on the Alaska megathrust: Geology, doi:10.1130/G35797.1.
Shiki, T., Tachibana, T., Fujiwara, O., Goto, K., Nanayama, F., and Yamazaki, T., 2008, Characteristic features of tsunamiites *in* Shiki, T., et al., eds., Tsunamiites—Features and implications: Amsterdam, Elsevier, p. 319–340, doi:10.1016/B978-0-444-51552-0.00018-7.
Smith, D.E., Cullingford, R.A., and Brooks, C.L., 1983, Flandrian relative sea level changes in the Ythan Valley, northeast Scotland: Earth Surface Processes and Landforms, v. 8, p. 423–438, doi:10.1002/esp.3290080504.
Soloviev, S.L., 1990, Sanak-Kodiak tsunami of 1788: Science of Tsunami Hazards, v. 8, p. 34–38.
Strasser, M., Moore, G.F., Kimura, G., Kitamura, Y., Kopf, A.J., Lallemant, S., Park, J., Screaton, E.J., Su, X., and Underwood, M.B., 2009, Origin and evolution of a splay fault in the Nankai accretionary wedge: Nature Geoscience, v. 2, p. 648–652, doi:10.1038/ngeo609.

Switzer, A.D., and Jones, B.G., 2008, Large-scale washover sedimentation in a freshwater lagoon from the southeast Australian coast: Sea-level change, tsunami or exceptionally large storm?: The Holocene, v. 18, p. 787–803, doi:10.1177/0959683608089214.

Szczuciński, W., Niedzielski, P., Kozak, L., Frankowski, M., Zioła, A., and Lorenc, S., 2007, Effects of rainy season on mobilization of contaminants from tsunami deposits left in coastal zone of Thailand by the 26 December 2004 tsunami: Environmental Geology, v. 53, p. 253–264, doi:10.1007/s00254-007-0639-4.

Szczuciński, W., Kokociński, M., Rzeszewski, M., Chagué-Goff, C., Cachao, M., Goto, K., and Sugawara, D., 2012, Sediment sources and sedimentation processes of 2011 Tohoku-Oki tsunami deposits on the Sendai Plain, Japan—Insights from diatoms, nannoliths and grain size distribution: Sedimentary Geology, v. 282, p. 40–56, doi:10.1016/j.sedgeo.2012.07.019.

Thio, H.K., Somerville, P., and Polet, J., 2010, Probabilistic tsunami hazard in California: Berkeley, University of California, Pacific Earthquake Engineering Research Center, PEER Report 2010/108, 330 p.

Tingstad, A.H., Moser, K.A., MacDonald, G.M., and Munroe, J.S., 2011, A ~13,000-year paleolimnological record from the Uinta Mountains, Utah, inferred from diatoms and loss-on-ignition analysis: Quaternary International, v. 235, p. 48–56, doi:10.1016/j.quaint.2010.11.023.

Tröels-Smith, J., 1955, Characterization of unconsolidated sediments: Dansk Geologiske Undersøgelse, ser. IV, v. 3, no. 10, 72 p.

Tuttle, M.P., Ruffman, A., Anderson, T., and Jeter, H., 2004, Distinguishing tsunami from storm deposits in eastern North America: the 1929 Grand Banks tsunami versus the 1991 Halloween storm: Seismological Research Letters, v. 75, p. 117–131, doi:10.1785/gssrl.75.1.117.

Vallier, T.L., Scholl, D.W., Fischer, M.A., Bruns, T.R., Wilson, F.H., von Huene, R., and Stevenson, A.J., 1994, Geologic framework of the Aleutian arc, Alaska *in* Plafker, G., and Berg, H.C., eds., The geology of Alaska: Boulder, Colorado, Geological Society of America, Geology of North America, v. G1, p. 367–388.

von Huene, R., Miller, J.J., and Weinrebe, W., 2012, Subducting plate geology in three great earthquake ruptures on the western Alaska margin, Kodiak to Unimak: Geosphere, v. 8, p. 628–645, doi:10.1130/ GES00715.1.

Vos, P.C., and de Wolf, H., 1988, Methodological aspects of paleo-ecological diatom research in coastal areas of the Netherlands: Geologie en Mijnbouw, v. 67, p. 31–40.

Vos, P.C., and de Wolf, H., 1993, Diatoms as a tool for reconstructing sedimentary environments in coastal wetlands; methodological aspects, *in* von dam, H., ed., Twelfth International Diatom Symposium: Hydrobiologia, v. 269/270, p. 285–296, doi:10.1007/BF00028027.

Waythomas, C.F., Watts, P., Shi, F., and Kirby, J.T., 2009, Pacific Basin tsunami hazards associated with mass flows in the Aleutian arc of Alaska: Quaternary Science Reviews, v. 28, p. 1006–1019, doi:10.1016/j.quascirev.2009.02.019.

Wintle, A.G., and Murray, A.S., 2006, A review of quartz optically stimulated luminescence characteristics and their relevance in single-aliquot regeneration dating protocols: Radiation Measurements, v. 41, p. 369–391, doi:10.1016/j.radmeas.2005.11.001.

Witter, R.C., Kelsey, H.M., and Hemphill-Haley, E., 2001, Pacific storms, El Niño and tsunamis: competing mechanisms for sand deposition in a coastal marsh, Euchre Creek, Oregon: Journal of Coastal Research, v. 17, p. 563–583.

Witter, R.C., Kelsey, H.M., and Hemphill-Haley, E., 2003, Great Cascadia earthquakes and tsunamis of the past 6700 years, Coquille River estuary, southern coastal Oregon: Geological Society of America Bulletin, v. 115, p. 1289–1306, doi:10.1130/B25189.1.

Witter, R.C., Hemphill-Haley, E., Hart, R., and Gay, L., 2009, Tracking prehistoric Cascadia tsunami deposits at Nestucca Bay, Oregon: Final technical report: U.S. Geological Survey, National Earthquake Hazards Reduction Program Award 08HQGR0076, 40 p., http://earthquake.usgs.gov/research/external/reports/08HQGR0076.pdf.

Witter, R.C., Briggs, R.W., Engelhart, S.E., Gelfenbaum, G., Koehler, R.D., and Barnhart, W.D., 2014, Little late Holocene strain accumulation and release on the Aleutian megathrust below the Shumagin Islands, Alaska: Geophysical Research Letters, v. 41, p. 2359–2367, doi:10.1002/2014GL059393.

Workman, W.B., 1966, Archaeological reconnaissance on Chirikof Island, Kodiak Group: A preliminary report: Arctic Anthropology, v. 3, p. 185–192.

Workman, W.B., 1969, Contributions to the prehistory of Chirikof Island, southwestern Alaska: [M.A. thesis]: Madison, University of Wisconsin, 1019 p.

Wright, D.C., 1964, Ocean cattle ranch: Alaska Sportsman, v. 30, no. 8–11, p. 36–37.

Wright, D.K., Forman, S.L., Waters, M.R., and Ravesloot, J.C., 2011, Holocene eolian activation as a proxy for broad-scale landscape change on the Gila River Indian Community, Arizona: Quaternary Research, v. 76, p. 10–21, doi:10.1016/j.yqres.2011.04.008.